Combining Silicon Photonics and Machine Learning for Red Blood Cell Characterization

Alexander P. Wende

A thesis

submitted in partial fulfillment of the

requirements for the degree of

Master of Science in Bioengineering

University of Washington

2018

Committee:

Daniel M. Ratner, Chair

Jill Johnsen

J. Nathan Kutz

Program Authorized to Offer Degree:

Bioengineering

University of Washington

Abstract

Combining Silicon Photonics and Machine Learning for

Red Blood Cell Characterization

Alexander P. Wende

Chair of the Supervisory Committee:

Associate Professor Daniel M. Ratner

Department of Bioengineering

Tens of millions of units of blood are transfused worldwide each year, with each individual unit requiring manual typing by a trained technician prior to transfusion. Several tools exist to help expedite the typing process, yet typing still remains a slow and costly process. In an effort to increase throughput and decrease costs of blood typing, recent work involving silicon photonic biosensors has demonstrated their potential as a rapid, low cost tool for typing blood. This thesis focuses on two separate aspects of silicon photonic blood typing: photonic sensor selection and validation along with automation of downstream data processing. Transverse electric and transverse magnetic mode microring resonators are compared for serologic and phenotypic typing assays. Phenotypic typing data from multiplexed photonic blood typing chips is used with several machine learning algorithms to predict blood types with accuracies rivaling by-hand analysis of the same data.

List of Figures

List of Tables

Table of Contents

Chapter 1. Introduction

1.A Research Objectives

The main objective of this MS thesis is to contribute to the development of rapid, low-cost silicon photonic biosensing assays for point-of-care ABO and RhD blood typing. The first half of this thesis focuses on different photonic devices that can be used for both forward and reverse blood typing. These devices, known as transverse electric and transverse magnetic mode microring resonators have differing strengths for biosensing, which are compared in the context of using both types of sensor to perform blood typing. The second half of this thesis focuses on how the analysis of data from multiplexed silicon photonic blood typing assays can be automated to further reduce the complexity of clinical blood typing. Multiple machine learning models are evaluated for use in automating this analysis, and insights into how this process may be further improved are discussed.

1.B Motivation and Background

1.B.1 Blood Typing

In 1901, Karl Landsteiner discovered the ABO blood group system and later, the Rh system[1]. The first successful human blood transfusion utilizing Landsteiner's blood typing techniques, based on red blood cell (RBC) agglutination, was performed in 1907, and at their core, blood typing techniques have remained largely unchanged since[2].

As Landsteiner discovered, humans express oligosaccharide antigens for groups A and/or B on the outer surface of their RBCs and typically have antibodies in their serum against the antigens not present on their cells (Figure 1-1). Blood type is traditionally defined by the presence of these surface antigens, with the four main types known as A, B, AB, and O. Many variant subtypes of the ABO system have been identified, having widely varying antigen structures and densities, as well as many different blood group antibodies. While these variant subtypes are more common than previously believed, they are not considered as commonly in transfusion medicine as the "canonical" ABO types[3].

In addition to the ABO blood group system, at least 34 other blood group systems have been identified, including the Rh system[4]. The Rh system has 49 known antigens, with the most important to transfusion medicine being D, C, c, E, and e. The RhD antigen, an transmembrane protein, is widely considered to be the second most important antigen system after ABO, with both ABO and RhD always being typed prior to any transfusion. As with the ABO system, RhD is typically characterized by a presence of either the antigen or antibodies against the antigen, but not both. When reporting the overall type of blood, the RhD type is commonly expressed as a plus or minus sign following the ABO type, as in AB+ or O-. A positive RhD type typically indicates the presence of the D antigen and the absence of an anti-D antibody, while a negative indicates the opposite.

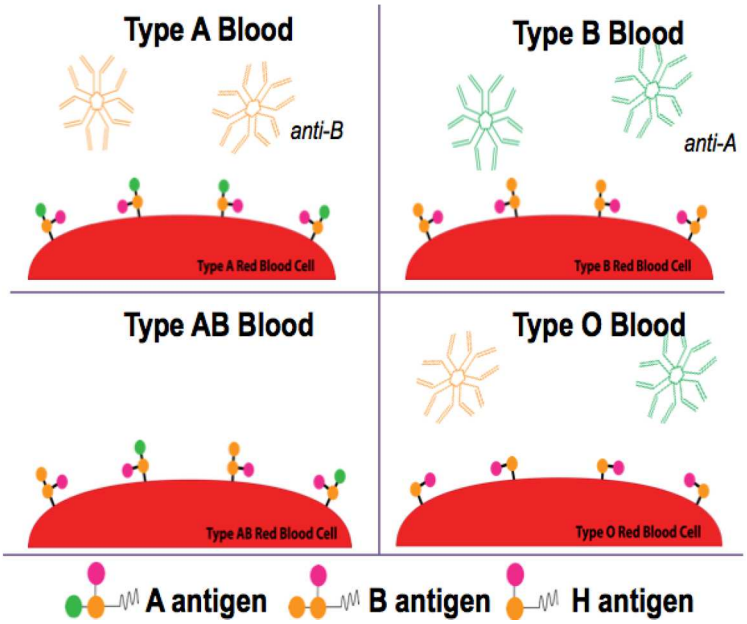

Figure 1-1 ABO blood groups in types A, B, AB, and O. The H antigen is a precursor to both the A and B antigen, and can be found on almost all RBCs.

Prior to transfusion, the ABO and RhD types of both the donor and recipient must be determined to avoid hemolytic transfusion reactions in the recipient. If the types aren't correctly matched, the recipient's antibodies can cause their immune system to attack the transfused blood, which may lead to clotting and potentially death. Several variations of Landsteiner's blood typing methods have been developed, but all common methods are still based on the agglutination of RBCs due to binding interactions between blood group antigens and antibodies. Because of the importance of determining the presence of both antibodies and antigens to prevent negative patient responses, two varieties of the standard blood typing test are used: forward and reverse.

For reverse typing, unknown plasma has reference RBCs of known type added to it. If the antibodies present in the plasma bind to the known antigens on the cells, aggregation occurs, with the antibodies binding several cells together into a visible clump. By adding RBCs of differing types in different tubes, all possible combinations of antigens and antibodies can be tested and compared to determine the overall type of blood. Similar to reverse typing, forward typing is also based on the aggregation of RBCs with serum antibodies. In forward typing, unknown RBCs are mixed with reagent antibodies, and as in direct typing, if the relevant antigen is present, visible clumping of cells occurs. The current gold standard test for both forward and reverse typing is to mix the different combinations of known and unknown RBCs and antibodies in test tubes, and to visually inspect the tubes for clumping. This test is slow, requiring as much as an hour for complete clumping of cells to occur. The reagents required are expensive, so a full typing panel can cost as much as $100 per unit of blood[5]. Some modern typing methods also require specialized equipment, constraining tests to being performed in well-equipped clinical labs, which further increases costs and slows time to result[6]. Finally, as measurement of cell aggregation is only semi-quantitative, a highly trained technician is required to evaluate the results of blood type testing. Together, these limitations prevent blood typing from being conducted at the point of care, which further complicates the transfusion workflow.

Many transfusions occur in trauma settings, where patients may need one or more transfusions immediately. Because a full typing panel can take up to an hour to complete, the type of a patient's blood often cannot be determined rapidly enough to guarantee a correct match. Since mismatched blood transfusions can cause serious complications, all trauma patients are given universal units of blood composed of O- RBCs and AB+ plasma. Because of the dependence on these universal units, shortages (especially of O- RBCs) are common all over the country. A rapid test with an easily interpretable result could be used at or near the patient's bedside, potentially reducing the dependence on universal units, in turn helping to reduce the strain on the medical system from blood shortages.

1.B.2 Silicon Photonics

Silicon photonics is a technology developed by the global telecommunications industry for high-speed communications and computation that has recently been adopted as a tool for biosensing. Silicon photonic biosensors typically consist of nanoscale photonic wires (known as waveguides) that serve as a medium for the propagation of near-infrared light. While the light is confined within the waveguide by total internal reflection, a portion of the light's energy travels outside the waveguide as an evanescent electric field that is sensitive to the refractive index of the medium surrounding the waveguide (Figure 1-2).

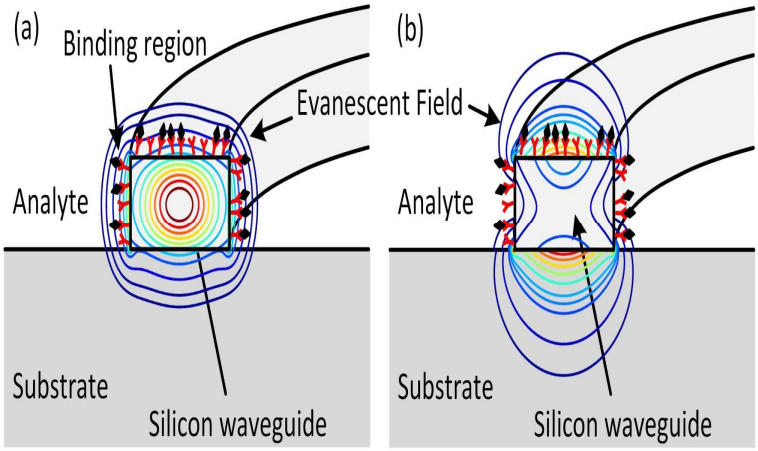

Figure 1-2 Evanescent field diagram of (a) transverse electric mode waveguide and (b) transverse magnetic mode waveguide

In order to increase the sensitivity of photonic biosensors, resonant structures such as rings[7] or disks[8] are added in close proximity to the waveguide. The resonant wavelength of such structures is dependent on the geometry and material of the structure, as well as the refractive index surrounding the structure[9]. Changes to this refractive index, typically due to a change in buffer or to molecular binding at the resonant structure's surface, result in a measurable change in the resonant wavelength of the sensor. This wavelength shift is positive for increases in refractive index and negative for decreases. Photodetectors can be used to quantify this shift relative to a baseline. Resonant wavelength changes plotted over time are known as sensorgrams, which is the standard format for interpreting photonic sensor data. By functionalizing these sensors with specific capture chemistries, each sensor can be used to detect the presence and binding of a different biomolecule in solution[10].

For silicon surfaces, the most common chemical functionalization strategy is passive adsorption of a binding protein. This strategy takes advantage of nonspecific protein binding to silicon surfaces. When a protein is exposed to a silicon surface, it will partially unfold, using the surface to help shield its

hydrophobic residues from the surrounding environment. Utilizing this property, silicon photonic biosensors can be coated with binding proteins such as streptavidin to provide a base for binding more specific capture reagents. Specialized inkjet printers can subsequently deposit sub-nanoliter sized droplets[11] of biotinylated capture reagents on specific sensors or groups of sensors on a silicon chip to produce multiplexed chips capable of performing multiple bioassays simultaneously.

In the studies presented here, several different photonic sensors were functionalized with a variety of blood typing reagents in order to compare different types of photonic sensors for blood typing applications and to demonstrate a proof-of-concept of simultaneous forward and reverse blood typing for ABO and RhD on a single multiplexed chip. Data from this proof-of-concept study was also used to train and evaluate several different machine learning models in order to demonstrate the possibility of automatic type reporting without the need for a trained technician.

Chapter 2. Transverse Electric and Magnetic Mode Ring Resonators for Erythrocyte and Serologic Phenotyping

2.A Abstract

More than 14 million blood transfusions occur annually in the United States, and each unit of donated blood must be thoroughly typed prior to transfusion. This testing typically occurs in clinical laboratories performed by specially trained technicians and is encumbered by reagent availability, cost, and time to result. A diagnostic platform capable of rapid and low-cost phenotyping of blood could improve workflows and reduce the reliance on universal donor blood units in inventory management. Silicon photonic biosensors represent an appealing platform to address the sensing needs for blood typing. In this study, we investigated the use of both transverse electric (TE) and transverse magnetic (TM) mode ring resonators for both serologic and phenotypic blood typing. TM mode rings were found to offer a two-fold surface sensitivity improvement over TE, and performed better for forward typing applications. However, TE and TM devices performed similarly for serologic typing assays. We demonstrated how both TE and TM ring resonators can support the determination of ABO phenotype of red blood cells and plasma for silicon photonic-enabled lab-on-chip applications in blood typing.

2.B Introduction

2.B.1 Silicon photonic biosensors

Silicon photonics is a chip scale technology that guides near-infrared light in nano-scale silicon wires known as waveguides. While high performance computing and data communication applications have driven the development of silicon photonic technologies[12-14], they also show promise for biosensing[15,16] and for lab-on-chip systems[17-19]. These devices operate using an electric field to detect molecular binding events on the waveguide's surface. The distribution of this electric field within the waveguide, referred to as the mode profile, depends on the light's polarization and wavelength, as well as the geometry and material properties of the waveguide. For a single mode waveguide, a portion of the electric field mode

profile resides outside the waveguide as an evanescent field. The evanescent field can be enhanced using a structure such as a ring or a disk to create a resonance condition within the waveguide[8]. This resonance condition greatly improves the sensitivity of the device, allowing it to be used as a biosensor.

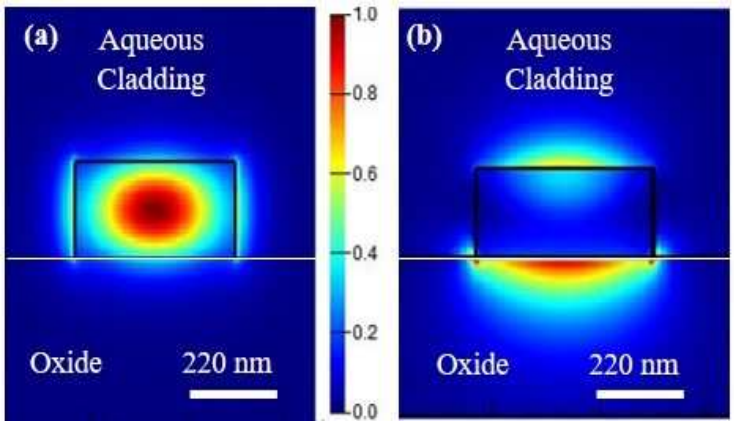

Figure 2-1 Simulated TE and TM mode profiles in silicon photonic waveguide cross-sections. (a) Fundamental TE mode profile in a 220 by 500 nm waveguide on buried oxide with aqueous cladding. (b) Fundamental TM mode profile in a 220 by 750 nm waveguide on buried oxide with aqueous cladding.

Figure 2-1 shows the electric field distribution for the fundamental transverse electric (TE) and transverse magnetic (TM) modes in a silicon waveguide on a silicon oxide substrate with aqueous cladding on the remaining three exposed sides. As biomolecules have a higher refractive index than that of the aqueous media in which they reside[20], molecules that bind to the waveguide's surface within the evanescent field, as shown in Fig. 2-2a and 2-2b, alter the propagation profile of the mode, namely loss and the effective refractive index, n_{eff}. For a ring resonator, the resonance condition is met when the optical length of the resonator, $2\pi R*n_{eff}$ (with R being the radius of the ring), is a multiple of the light's wavelength[7]. A change in the effective index caused by a molecular binding event will shift the wavelength accordingly (see Fig. 2-2c). These wavelength changes can be quantified using a tunable laser and power meter. If these changes are continuously tracked over time, they can be displayed as a sensorgram similar to the one shown in Figure 2-2d.

The sensitivity of these resonant sensors is largely dependent on the overlap with the analyte. From Fig. 2-1, it is expected that a TM mode will be more sensitive than a TE mode, as a greater portion of the mode overlaps with the aqueous cladding and binding region. However, due to the corresponding increase in absorption loss in the aqueous cladding for the TM mode, the intrinsic limit of detection remains constant[8].

While silicon photonic biosensors have been demonstrated for detection of proteins[21, 22], nucleic acids[23], viruses[24], and bacteria[25], their ability to perform serologic (also referred to as reverse, back, or indirect) and phenotypic (also referred to as forward, front, or direct) blood typing has only recently been demonstrated by our group. In this study, we describe the design, fabrication, and characterization approaches of both TE and TM mode rings. We also compare the performance of both types of rings for serologic and phenotypic typing assays using human blood samples.

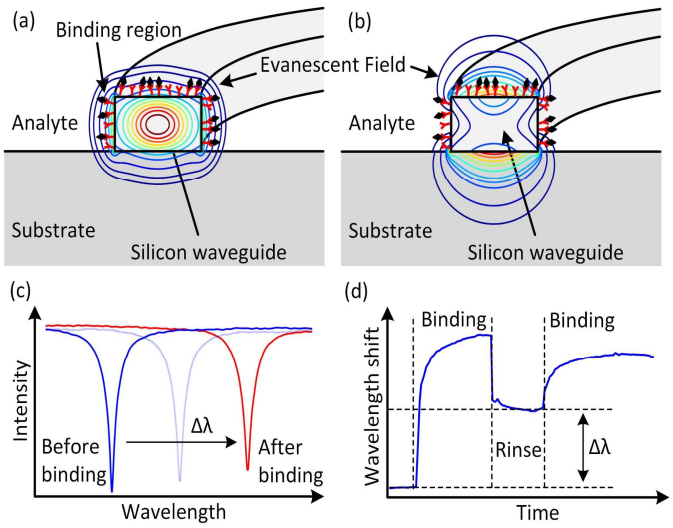

Figure 2-2 TE and TM mode biosensor principles of operation. Electric field intensity of a fundamental (a) TE and (b) TM mode profile in a silicon ring resonator waveguide showing the evanescent field overlap with the substrate (silicon oxide) and bound biomolecules in aqueous cladding. (c) Example of the resonant wavelength shift resulting from a change in effective refractive index due to the adsorption of biomolecules. (d) Sensorgram of resonant wavelength shift tracked over the course of a reverse blood typing assay. The permanent wavelength shift after the rinse step indicates molecular adlayers bound to the waveguide's surface.

2.B.2 Blood typing

The blood group antigens present on the surface of red blood cells define a patient's blood type, with the process of identifying the presence and/or absence of these antigens known as blood typing. The most familiar red blood cell antigen systems include ABO and RhD[26] (+/-). Identification of these antigens is paramount to transfusion medicine, as they give rise to naturally occurring alloantibodies against the antigens absent from the host's red blood cells[26] (RBCs). Hemolytic transfusion responses due to unmatched blood between donors and recipients account for approximately 25% of fatalities associated with transfusion errors[27]. As such, it is necessary to accurately establish blood type compatibility between donors and recipients prior to transfusion.

While many approaches to blood typing exist, tube-based agglutination assays remain the current gold standard[28]. Agglutination assays can either measure the blood type directly by detecting blood group

antigens, or indirectly by detecting blood group antibodies. These two assays are referred to as forward typing and reverse typing. For forward typing assays, antigen specific IgM antibodies are introduced into a saline solution with suspended RBCs of unknown type. Through antibody binding, the RBCs aggregate and precipitate, indicating the presence of the antigen. For reverse typing, special reference RBCs of known type are added to a serial dilution of plasma. Agglutination indicates the presence of the blood group specific antibodies. For both cases, a trained technician observes the result and rates the agglutination semi-quantitatively on a scale of 0 (no agglutination) to 4+ (strong agglutination).

In 2013, more than 14 million units of whole blood were collected for transfusions in the United States[29]. Each of these units underwent forward and reverse typing to determine the blood type for both the ABO and RhD groups. A bench top, near-bedside, multiplexed diagnostic platform capable of simultaneously performing serologic and phenotypic typing for each relevant blood group could improve work flows, time to result, and cost, while also minimizing the chance of transfusion errors (e.g. wrong blood in tube errors).

Multiplexed platforms utilizing microarrays and SPR have been investigated for blood typing[28, 30-33] but have yet to be extended to the full panel of tests required. Bonanno et al. used a porous silicon, label-free optical biosensor to detect rabbit IgG from whole rabbit blood with minimal sample preparation, but did not demonstrate the detection of RBC antigens directly[34]. The use of next-generation sequencing for predicting antigen phenotypes has also been investigated[35, 36]. The main

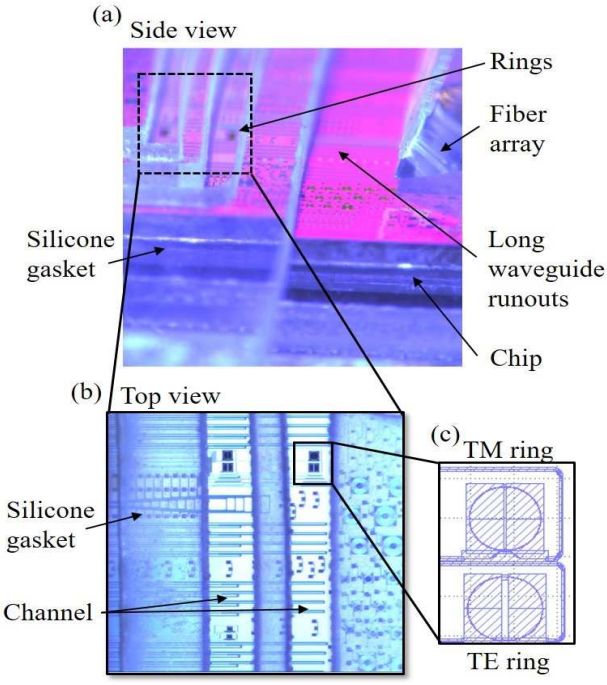

Figure 2-3 TE and TM mode rings in fluidic channels. (a) Side view showing the fiber array used to couple light on and off the chip, the long waveguide runouts, and the sensors in silicone gasket channels. (b) Overhead photograph showing both sets of TE and TM mode rings in separate channels. (c) Graphic data system image showing the layout of the TE and TM mode rings.

drawback with this approach is that ABO blood group genes do not directly produce surface antigens, but instead encode glycosyltransferases that in turn determine the oligosaccharide epitopes of the surface antigens. Rare alleles lead to slight glycosyltransferase variations, which ultimately impart antigen phenotypes[26, 37].

	TE ring	TM ring	units
Waveguide width	500	750	[nm]
Coupling length	7.24	3	[μm]
Optical path length	265.81	257.33	[μm]
Surface area	168.67	229.36	[μm^2]

Table 2-1 Summary of design parameters for TE and TM mode rings.

2.C Methods and Materials

2.C.1 Sensor design and fabrication

Ring resonators were developed using methods described in Bogaerts et al.[7]. All designs assumed a 220 nm thick silicon waveguide on 2 μm of silicon oxide. MODE Solutions (Lumerical; Vancouver, Canada) was used to simulate modal fields in 2D waveguides while custom MATLAB scripts were used to determine ideal waveguide coupling gaps and lengths. Table 2-1 summarizes design parameters for both TE and TM mode rings. Figure 2-3 shows the fabricated devices and their layouts.

Photonic rings were fabricated through a CMOS foundry compatible fabrication process (deep-UV lithography, 193 nm) offered through ePIXfab (IMEC; Leuven, Belgium). The multi-project wafer (MPW) was organized by CMC Microsystems. Waveguides were patterned onto 220 nm thick crystalline silicon on top of wavers with 2 μm of silicon oxide.

Chips were cladded with a polymer cladding (CYTOP, AGC Chemicals; Exton, PA) to improve durability and reusability, as well as to reduce optical losses in the long waveguide runouts between the vertical grating I/O couplers and biosensors. CYTOP is a perfluoropolymer with high chemical resistance and useful optical properties, with over 95% light transmittance through deep ultra-violet (DUV) to near-infrared (NIR) range, as well as a refractive index of 1.34. Openings in the cladding were created in order

to expose biosensors to the aqueous environment[38]. Laser-cut silicone gaskets were used to create fluidic channels over the TE and TM mode sensors (Figure 2-3).

2.C.2 Sensor characterization

Bulk sensitivity was assessed in an aqueous environment using refractive index standards made from ultra-pure deionized water (Barnstead Nanopure, Thermo Scientific) and sodium chloride (NaCl, Acros Organics, Thermo Fisher Scientific). Solutions of 62.5 mM, 125 mM, 250 mM, 500 mM, and 1 M NaCl were degassed under vacuum in an ultrasonic bath (VWR B2500A-MTH), and their refractive indices were measured using a Reichert AR200 digital refractometer (Depew, NW).

Surface sensitivity was characterized via layer-by-layer adsorption of electrostatically charged polymers, as demonstrated by Bailey *et al.*[39]. Prior to characterization, sensors were cleaned with Piranha solution (3:1 hydrogen peroxide: sulfuric acid by volume) then rinsed with deionized water. Following cleaning, sensors were exposed to polyethylenimine (PEI, 5 mg/mL), a positively charged polymer which acts as an anchor for subsequent bilayers. Next, solutions of negatively charged polystyrene sulfonate (PSS, 5 mg/mL) and positively charged poly(allylamine hydrochloride) (PAH, 5 mg/mL) were alternately sequenced across the sensor to create bilayers reported to be 3±0.2 nm thick[39]. Following the exposure of the sensors to each electrostatic polymer solution, Tris buffer (0.5 mM, 100 mM NaCl, pH 7.1) was used to rinse unbound polymer from the fluidics, preventing precipitation and clogging.

In order to measure susceptibility to temperature variation, multiple wavelength sweeps were performed in an aqueous environment while thermally tuning chips. Peaks were tracked and averaged in a similar manner to bulk sensitivity measurements.

2.C.3 Modeling and experimental validation

Waveguide mode profiles were determined using MODE Solutions (Lumerical, Canada) in order to help validate the observed performance metrics and adsorbed film thickness in biosensing assays. For TE sensors, the computational model consisted of a 220 nm by 500 nm silicon waveguide on buried oxide

with aqueous cladding. TM mode sensors were simulated with a 220 nm by 750 nm waveguide in the same conditions. Bulk sensitivity for both waveguide geometries were simulated by performing frequency sweeps using measured refractive index values from the NaCl refractive index standards. Surface sensitivity experiments were validated by simulating adlayers with a refractive index of 1.68 in 10 nm increments up to 200 nm with a background cladding similar to water (n = 1.333)[39]. Surface sensitivity prediction towards biofilms were determined by simulating protein adlayers with a refractive index of 1.48[21, 40] in 10 nm increments up to 200 nm with a background cladding similar to water (n = 1.333).

2.C.4 Blood typing reagents

Bovine serum albumin (BSA) and streptavidin (SA) were purchased from Sigma Aldrich (St. Louis, MO, USA). DryCoat Assay Stabilizer was purchased from Virusys Corporation (Taneytown, MD, USA). For forward typing assays, biotinylated goat anti-mouse IgM antibodies were purchased from Thermo Fisher Scientific (Rockford, IL, USA). Murine IgM anti-A and anti-B antibodies were provided by Merck, Millipore. A phenotypic typing capture reagent mix was prepared by incubating a 1:1 molar ratio of biotinylated goat anti-mouse IgMs with either mouse anti-A or anti-B IgM at 4 °C for one hour. Biotinylated anti-glycophorin A IgG antibodies were purchased from Miltenyi Biotec (San Diego, CA, USA) and used in separate experiments as a positive control for phenotypic typing of red blood cells.

For serologic typing assays, monoclonal A and B typing antibodies were purchased from Immucor (Norcross, GA, USA). Biotinylated multivalent polyacrylamides containing blood group antigens A and B (PAA-A and PAA-B) were purchased from GlycoTech (Gaithersburg, MD, USA). The same biotinylated polyacrylamide polymer without either antigen (PAA) was also purchased and used as a negative control. Goat anti-mouse IgM and murine anti-human IgG/A/M antibodies for secondary amplification were purchased from Thermo Fisher Scientific (Rockford, IL, USA).

Freshly drawn human blood samples stored in an appropriate anticoagulant at 4 °C were obtained in collaboration with Dr. Jill Johnsen of the Bloodworks Northwest Research Institute (Seattle, WA, USA). Whole blood samples were centrifuged at 2000 G for 10 minutes at 4 °C. Following centrifugation, the plasma and buffy coat layers were removed from the cell pellet and stored separately. Undiluted human plasma was analyzed directly while whole red blood cells were analyzed in a 1:10 dilution in phosphate buffered saline (PBS).

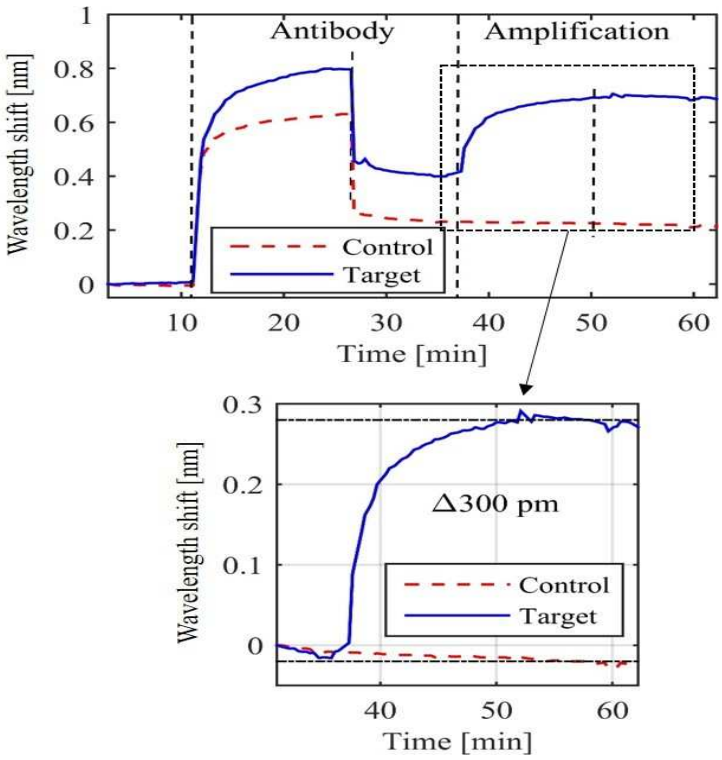

Figure 2-4 Example of a reverse typing reagent validation assay. The inset shows the reference subtracted secondary amplification step, with a 300 pm wavelength offset.

2.C.5 Reagent validation

RBC antigenicity was validated using a standard agglutination assay with commercially available monoclonal A and B typing IgM antibodies purchased from Immucor (Norcross, GA). Capture antibody specificity was validated by comparing the sensor responses from RBCs binding to specific capture antibodies with sensor responses from RBCs binding to an anti-glycophorin A positive control antibody. For reverse typing assays, the PAA-A and PAA-B polymers had their antigenicity validated using commercially available anti-A and anti-B IgM antibodies from Immucor. Figure 2-4 shows an example of an reverse typing validation assay on TE/TM mode rings. The large signal difference between the target and control during the amplification step confirms the antigenicity of the PAA-A/B polymers.

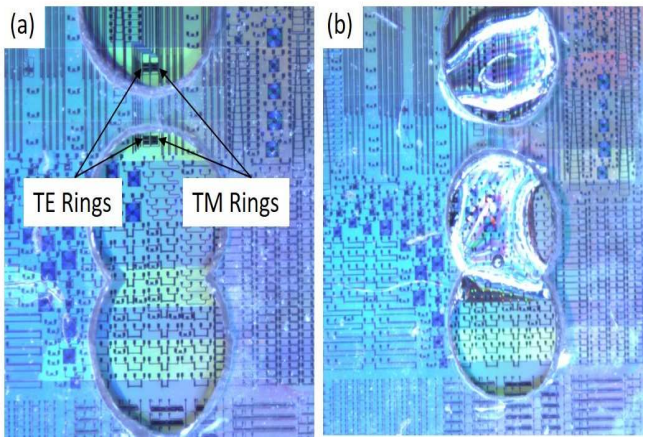

Figure 2-5 Spotting of functionalization reagents. (a) Photograph of the 500 µm thick silicone spotting gasket positioned over sets of TE and TM mode rings. (b) 250 nL droplets of biotinylated typing reagents (PAA-A or PAA-B for reverse typing, conjugated antibody complexes for forward typing) for functionalization of streptavidin-coated sensors.

2.C.6 Sensor functionalization

For both forward and reverse typing assays, streptavidin (0.1 mg/mL) was passively adsorbed to the sensors' surfaces for at least three hours at room temperature. Chips were then rinsed with PBS and blown dry using filtered air. A laser-cut silicone gasket was then placed on each chip to form two separate wells for functionalization, as shown in Figure 2-5.

For forward typing, one well was spotted with the anti-A capture reagent mix, and the other well was spotted with the anti-B capture reagent mix. For reverse typing, one well was spotted with biotinylated PAA-A, and the other well was spotted with biotinylated PAA-B. Both types of chips were then incubated in a humid environment for one hour at room temperature. Following incubation, chips were thoroughly rinsed with PBS, and subsequently blocked with 1 mg/mL BSA in PBS for 20 minutes. The chips were then rinsed again, dipped in DryCoat, and blown dry. Chips were stored dry in a refrigerator until use.

2.C.7 Test platform

A custom fiber-array based probe station, built by our group, enabled the automated testing and characterization of photonic devices. Figure 2-6 shows a picture of the main stage and two channel flow cell used for characterization and biosensing assays. A syringe pump (not shown)

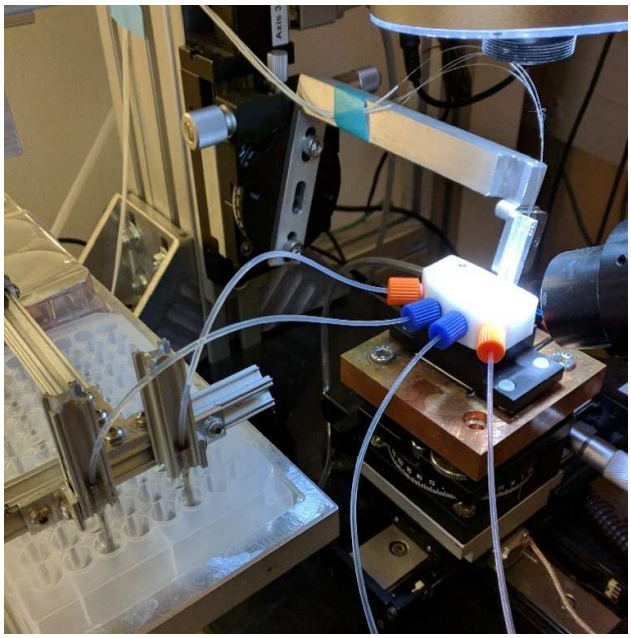

Figure 2-6 Photograph of the automated probe station

sequences reagents from two well plates mounted on a motorized stage. In addition to test platform hardware, our custom analysis software was used to help analyze acquired datasets. This analysis tool includes features such as peak fitting, reference channel subtraction, and sensorgram signal difference measurements.

2.D Results and Discussion

2.D.1 Sensor characterization

Due to the lack of widely accepted standard performance metrics for refractive index-based sensors, we chose several objective measures to compare the performance of our silicon photonic biosensors including sensitivity, quality factor, and limit of detection[41-43]. As sensitivity is defined as a change in resonant wavelength (λ_{res}) relative to a change in one of several environmental factors, we divided sensitivity into three independent metrics based on different environmental factors: bulk sensitivity, surface sensitivity, and temperature sensitivity.

2.D.1.1 Bulk sensitivity (S_{bulk}) describes how a change in the refractive index of the sensor's cladding impacts the resonant wavelength of the sensor. S_{bulk} is defined as

$$S_{bulk} = \frac{\Delta\lambda_{res}}{\Delta n_{clad}} = \frac{\lambda_{res}}{n_g}\left(\frac{\delta n_{eff}}{\delta n_{clad}}\right)_{\lambda_{res}, n^0_{clad}}$$

In order to predict the bulk sensitivity of the fundamental TE mode, we performed MODE simulations with a 220 by 500 nm waveguide. The same simulations

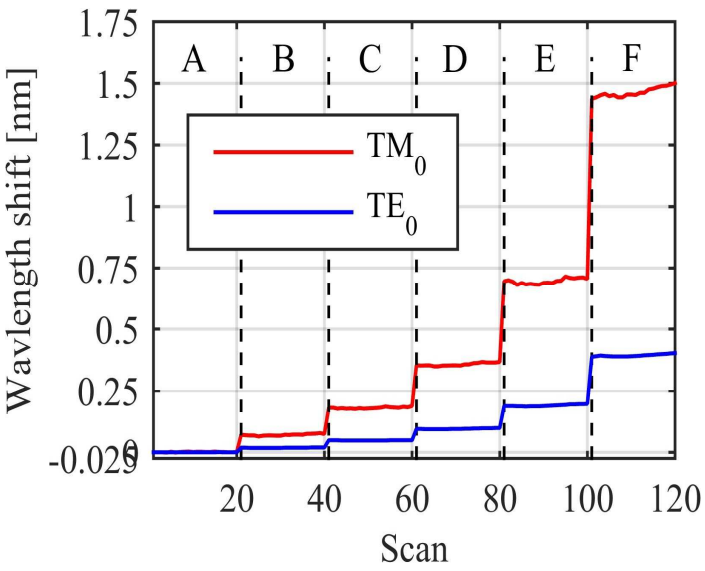

Figure 2-7 Sensorgram of TE and TM mode ring resonator wavelength shifts when exposed to NaCl refractive index standard solutions. Bulk sensitivity was determined by the slope of a best-fit line of the average wavelength at each step relative to the NaCl concentration of the step.

were performed with a 220 by 750 nm waveguide to predict the bulk sensitivity of the fundamental TM mode. Simulated models suggest a bulk sensitivity of 44.7 nm/RIU (refractive index unit) for the TE mode and 146.6 nm/RIU for the TM mode. These simulations used an aqueous environment and a central wavelength of 1505 nm.

S_{bulk} was determined experimentally by sequencing a two-fold serial dilution of 1M NaCl across TE and TM mode ring resonators while monitoring resonant wavelength. Figure 2-7 shows the observed resonant wavelength shifts as different concentrations of NaCl are exposed to TE and TM mode rings. The slope of these shifts relative to NaCl concentration determines the bulk sensitivity of a ring resonator. We observed bulk sensitivities of 41.2 ± 1.6 nm/RIU for TE mode rings, and 146.8 ± 2.5 nm/RIU for TM mode rings. Bulk sensitivity measurements were performed in triplicate and agree with the simulated values.

2.D.1.2 Surface sensitivity ($S_{surface}$) represents resonant wavelength change in response to the addition of molecular adlayers onto the surface of a waveguide. This is important for biosensing applications involving the adsorption of biomolecular adlayers. Protein adlayers have been reported to exhibit a refractive index of 1.48[21, 40] and to form 1-3 nm adlayers on a native oxide surface[44-47]. Therefore, a waveguide's resonant wavelength response ($\Delta\lambda_{res}$) to homogeneous protein adlayers can be calculated using

$$\Delta\lambda_{res} = \frac{\lambda_{res}}{n_g}\left(\frac{\delta n_{eff}}{\delta t}\right)_{t_0}$$

where t is molecular layer thickness, n_g is the group index, n_{eff} is the mode's effective refractive index, and λ_{res} is the resonant wavelength. To better understand the optical response to adsorbed molecular films during blood typing assays, we performed MODE simulations on TE and TM mode waveguides. Simulations using refractive index adlayers (n=1.68) to mimic alternating electrostatic polymer layers were compared to the experimentally observed results.

Simulations were also run with refractive index layers similar to protein adlayers (n=1.48). Figure 2-8a shows the simulated results for protein adlayers up to 200 nm thick. While both TE and TM mode waveguides approach horizontal asymptotes as layer thickness increases, TM waveguides offered improved sensitivity to thicker protein adlayers due to their larger evanescent field overlap with the surrounding environment[8]. Figure 2-8b shows the decrease in surface sensitivity as adlayer thickness increases. The ratio of these surface sensitivities is plotted as well, revealing that TM waveguides offer a 2x sensitivity improvement at the waveguide surface and a 3x improvement for a 30 nm-thick protein adlayer. Based on the biomolecules involved in the blood typing assays discussed herein, we expect protein films ranging from 10 to 50 nm thick[48-50]. The ratio of wavelength shifts for TE and TM ring resonators can be used to help elucidate the biofilm thickness in an assay, assuming both sensors have identical functionalization and are exposed to the same biological sample.

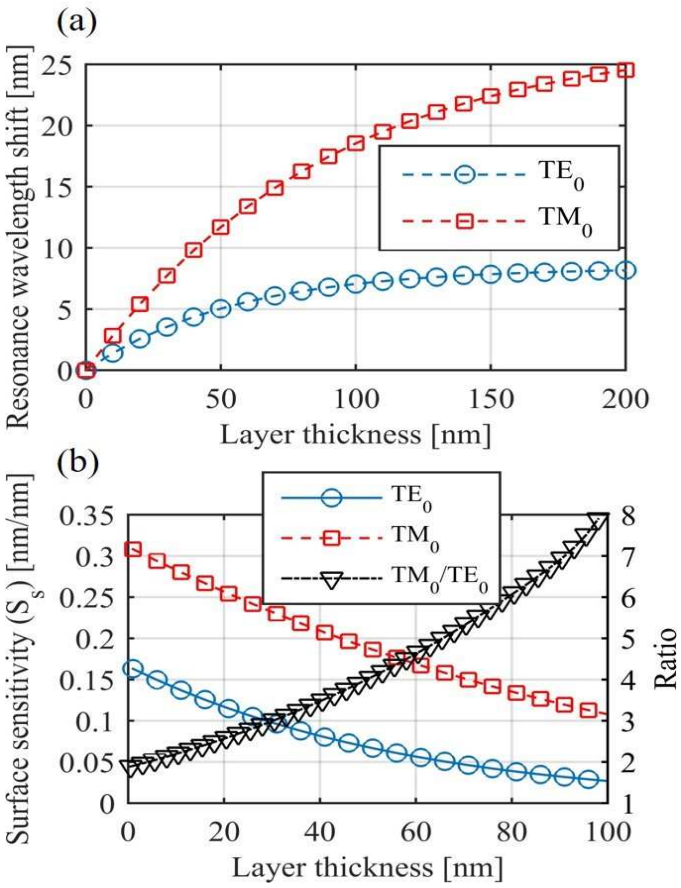

Figure 2-8 Surface sensitivity simulation results for TE and TM mode resonators. (a) Relative resonant wavelength shifts in response to increased thickness of a simulated homogeneous protein adlayer (n = 1.48 with aqueous background cladding of n = 1.33). (b) Surface sensitivities calculated by normalizing resonant wavelength shifts relative to adlayer thickness. Surface sensitivity ratio of TM to TE is plotted in black relative to adlayer thickness.

2.1.3. Temperature sensitivity (S_{temp}) represents the change in resonant wavelength in response to changes in the local temperature of the sensor. This is an important system-design consideration for biosensors, as thermal drift can greatly increase signal noise. Thermal control of the chip during measurement can be

used minimize thermal drift, but in non-thermally controlled systems, assay detection limits can be negatively impacted. To characterize temperature sensitivity, resonant wavelengths for TE and TM mode ring resonators were monitored while thermally tuning the system between 15 and 40 °C. Measurements were performed in an aqueous environment on three TE and three TM mode rings across three different chips. We observed a temperature sensitivity of 70 ± 0 pm/K for TE mode rings, and 39.8 += 0.75 pm/K for TM mode rings. The high temperature sensitivity of TE mode rings can be explained by the majority of TE modes existing within the silicon waveguide (Figure 2-1), which has greater thermal conductivity than the aqueous cladding surrounding the waveguide. TM mode rings have much less mode overlap with the waveguide, with the majority of TM modes existing in the aqueous cladding, thereby reducing temperature sensitivity. The lower temperature sensitivity of TM mode rings indicates a greater resistance to thermal noise than that of TE mode rings.

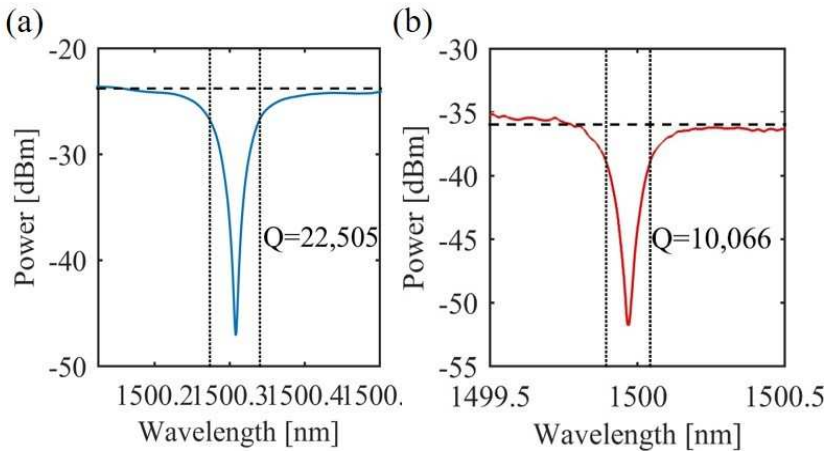

Figure 2-9 Measured resonant peak width used to approximate resonator Q for (a) TE and (b) TM mode rings.

2.1.4. Quality factor (Q) is a measure of the average number of round trips a photon makes while inside a resonator. This is a dimensionless number based on the resonator's loss and the index of refraction of the resonator material[41]. Q can be approximated experimentally by dividing the wavelength of a resonant peak (λ_{res}) by the peak's full width at half maximum (FWHM). Figure 2-9 shows the resonant peaks used to calculate Q for the TE and TM sensors. Higher Q's reduce a sensor's spectral noise[43] and improve its intrinsic limit of detection (iLoD). The iLoD can be understood as the minimum refractive index change

required to shift the resonance wavelength by one resonator line width[8, 51] ($\delta\lambda_{3dB}$). Algebraically, the iLoD is defined as,

$$iLoD = \frac{\lambda_{res}}{Q \bullet S}$$

where λ_{res} is the sensor's resonant wavelength in nm, Q is the dimensionless quality factor of resonator, and S is the bulk sensitivity in nm/RIU. Using the FWHM approximation for Q, the fabricated TE rings exhibit a Q of 22.5×10^3 and an iLoD of 1.6×10^{-3} [RIU]. The TM rings have a Q of 10.1×10^3 and an iLoD of 1.0×10^{-3} [RIU].

	TE Meas. (Sim.)	TM Meas. (Sim.)	Units
Sbulk	41.2 (44.7)	146.75 (146.6)	[nm/RIU]
Ssurface	(0.16)	(0.31)	[nm/nm]
Stemp	70 (67)	39.8 (38)	[pm/K]
Q	22.5k	10.1k	[]
iLoD	$1.6\cdot10^{-3}$	$1.0\cdot10^{-3}$	[RIU]

Table 2-2 Summary of experimental and simulated (sim.) measures of performance for fabricated 1550 nm wavelength TE and TM mode ring resonators

Table 2-2 summarizes the various measures of performance for the fabricated TE and TM mode ring resonators used in this work. The increased bulk and surface sensitivities of the TM mode ring are expected, as more of the evanescent field overlaps with the surrounding aqueous environment. For the same reason, TM mode rings also have more absorptive loss the TE mode rings, resulting in a lower Q. For both types of resonator, bulk sensitivity and temperature sensitivity closely match simulated values. Based on these performance metrics alone, the TM mode rings are expected to provide enhanced sensitivity for blood typing.

2.D.2 Reverse typing

Reverse blood typing involves the detection of serum or plasma blood group isohemagglutinins. Figure 2-10 shows a schematic representation of the steps involved in functionalizing sensors and performing reverse typing assays. Methods for sensor functionalization are described in detail in section 2.C.6 and depicted in Fig 2-10. For reverse typing assays, sensors were subjected to undiluted human plasma

followed by a PBS rinse (Fig. 2-10d). A secondary amplification antibody (anti-human IgG/M/A) is used to amplify the presence of bound anti-A and anti-B antibodies (Fig. 2-10e) in order to improve the signal-to-noise ratio.

Each fabricated photonic chip has four ring resonators, two TE and two TM. For reverse typing, one of each ring type is functionalized with polymeric blood group A and B antigen trisaccharides (PAA-A or PAA-B). In order to characterize non-specific binding, the other two rings are functionalized as negative controls with polyacrylamide polymers without antigens (PAA). For analysis, a reference

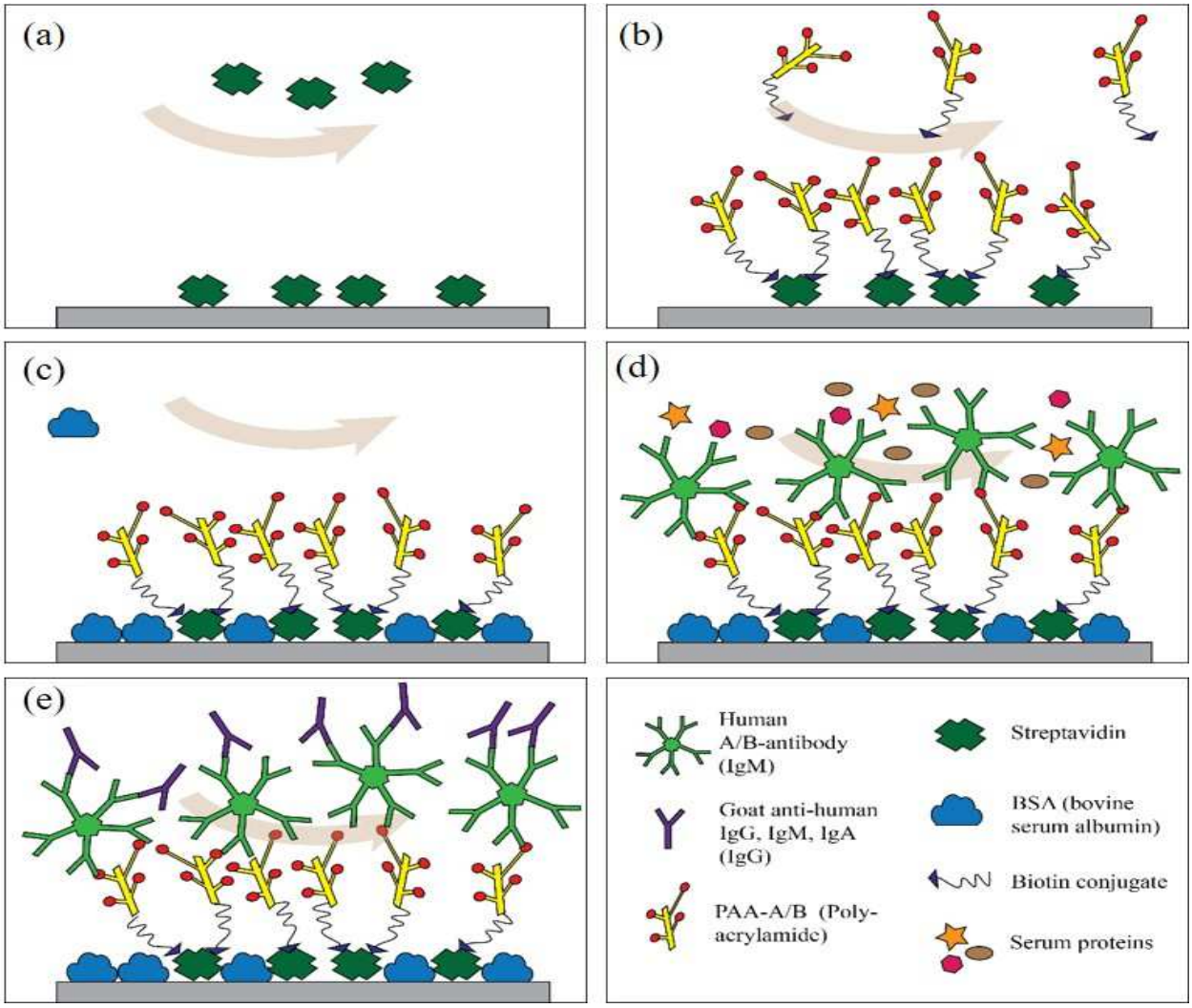

Figure 2-10 Schematic representing the steps involved with reverse typing assays. (a) Streptavidin is passively adsorbed to sensors. (b) Binding of biotinylated multivalent polyacrylamides with A and B blood group antigen trisaccharides (PAA-A and PAA-B) to the streptavidin coated surface. (c) Blocking any remaining exposed surfaces on the sensor using BSA. (d) Introduction of undiluted human plasma samples and binding of antibodies to the surface-bound antigens. (e) Signal amplification using an anti-human IgG/IgA/IgM antibody. Steps (a)-(c) were conducted off-line while steps (d)-(e) were performed during the assay.

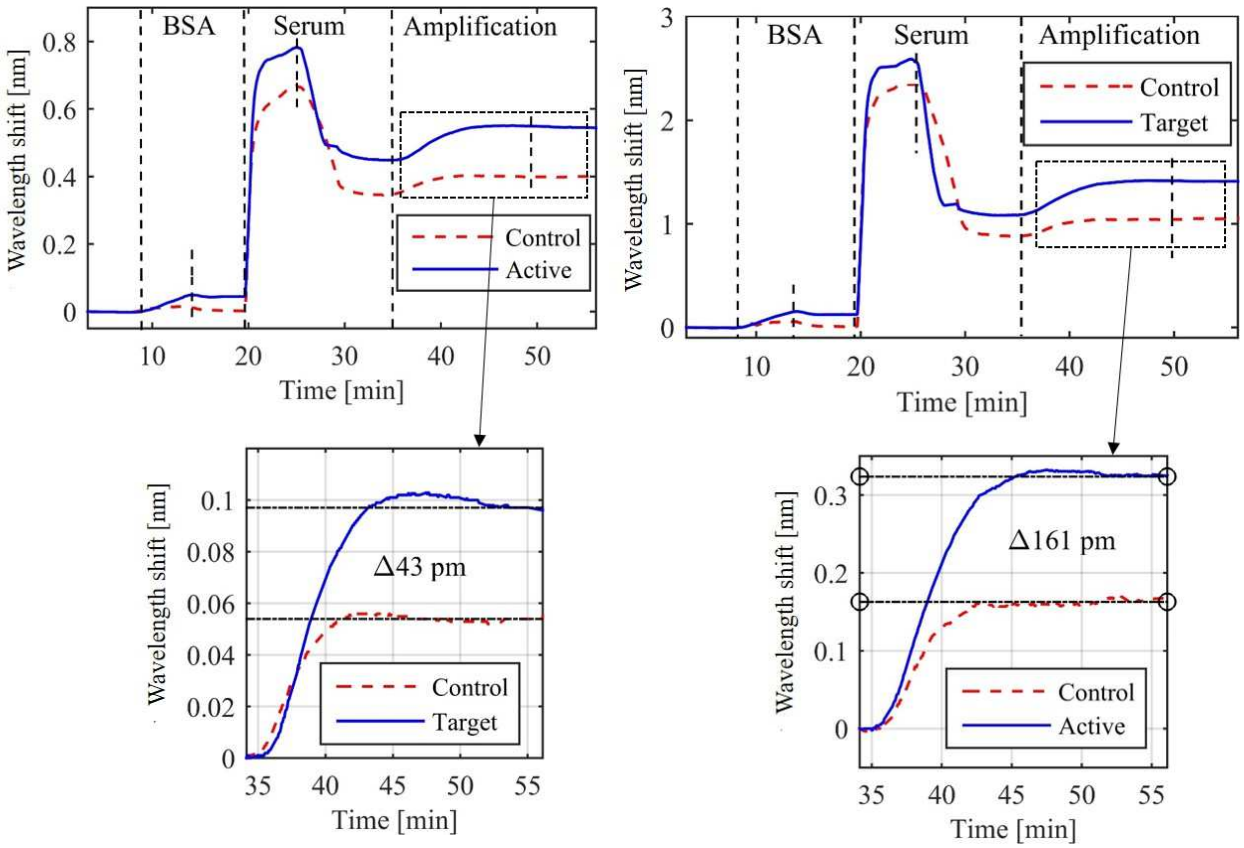

Figure 2-11 Reverse typing results of type-A plasma on (a) TE and (b) TM mode microring resonators functionalized with PAA-B.

subtraction is performed by subtracting the wavelength shift of the control ring from the wavelength shift of the target ring. The difference in resonance wavelength shifts after the secondary amplification indicates the specific binding isohemagglutinins from human plasma samples to the functionalized sensors. Figure 2-11 shows the acquired sensorgrams for a reverse typing assay of type-A plasma using TE and TM mode rings. Figure 2-12 shows the acquired sensorgrams for a reverse typing assay of type-B plasma using TE and TM mode rings. Figure 2-11a shows signal response using TE mode ring while Fig. 2-11b shows the results using TM mode rings. In both plasma samples, a large shift in resonance wavelength observed in the sensorgrams during plasma exposure results from the matrix effect of plasma that consists of a multitude of proteins, which in turn cause a significant fouling of these residual proteins on the sensor's surface despite a subsequent PBS rinse to remove excess, unbound molecules. In order to improve upon the signal-to-noise response, anti-human IgG/A/M was used as a secondary antibody that specifically captures isohemagglutinins and alloantibodies bound to the sensors during plasma exposure.

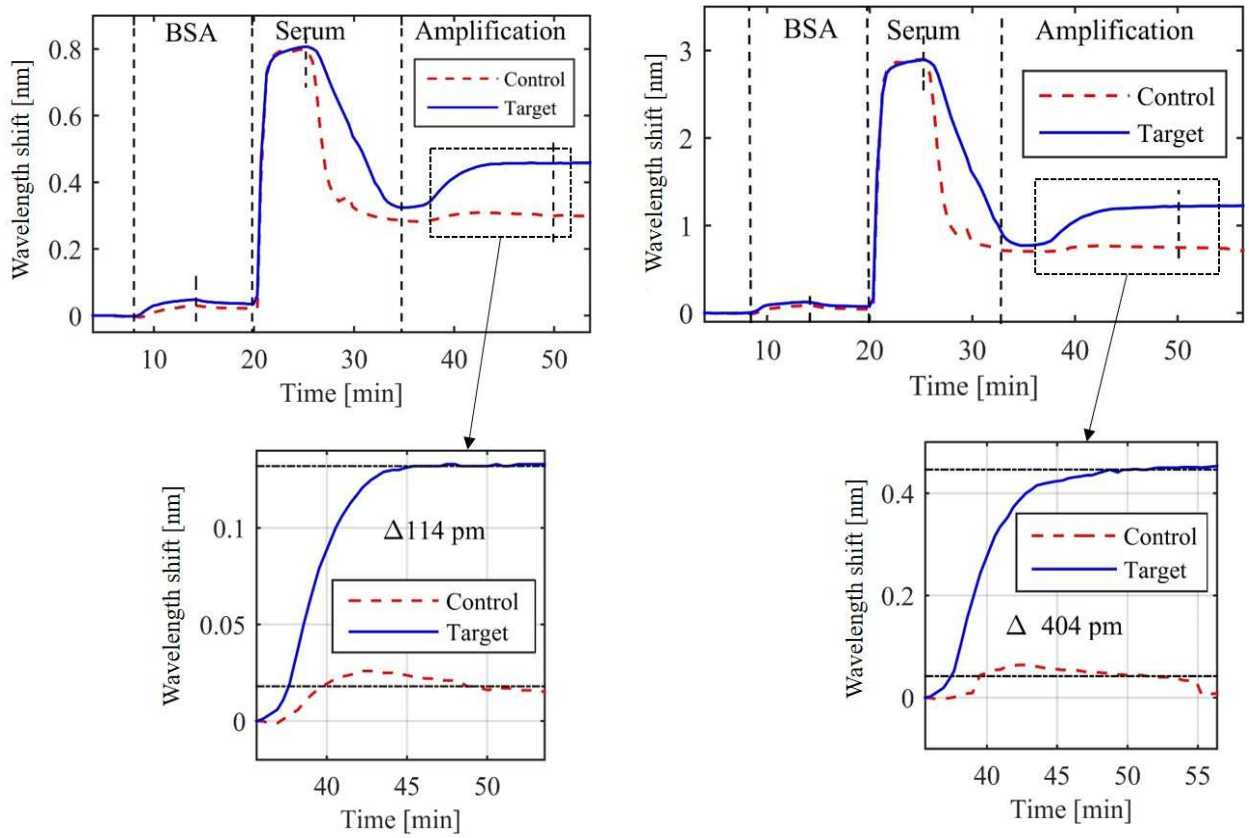

Figure 2-12 Reverse typing results of type-B plasma on (a) TE and (b) TM mode microring resonators functionalized with PAA-A.

As expected, a TM mode ring exhibits a nearly 4-fold improvement on signal amplification in both type-A and B plasma samples. The differential resonance wavelength shifts during secondary amplification of bound anti-B antibodies in type A plasma are 43 pm and 161 pm for TE and TM mode rings, respectively (Fig. 2-11 insets). Consistently with type-A plasma, the differential wavelength shifts during secondary amplification of bound anti-A antibodies are 114 pm and 404 pm for TE and TM mode rings, respectively (Fig. 2-12 insets). Given that the sensors were simultaneously functionalized and tested using the same plasma sample for each assay, this significant improvement in sensitivity is inherit to TM mode ring's larger sensing surface area than that of the TE mode ring.

2.D.3 Forward typing

In contrast to indirect typing, direct blood typing is an assay performed to detect the presence of blood group antigens on the red blood cell surface. Figure 2-13 shows a schematic representation of the steps

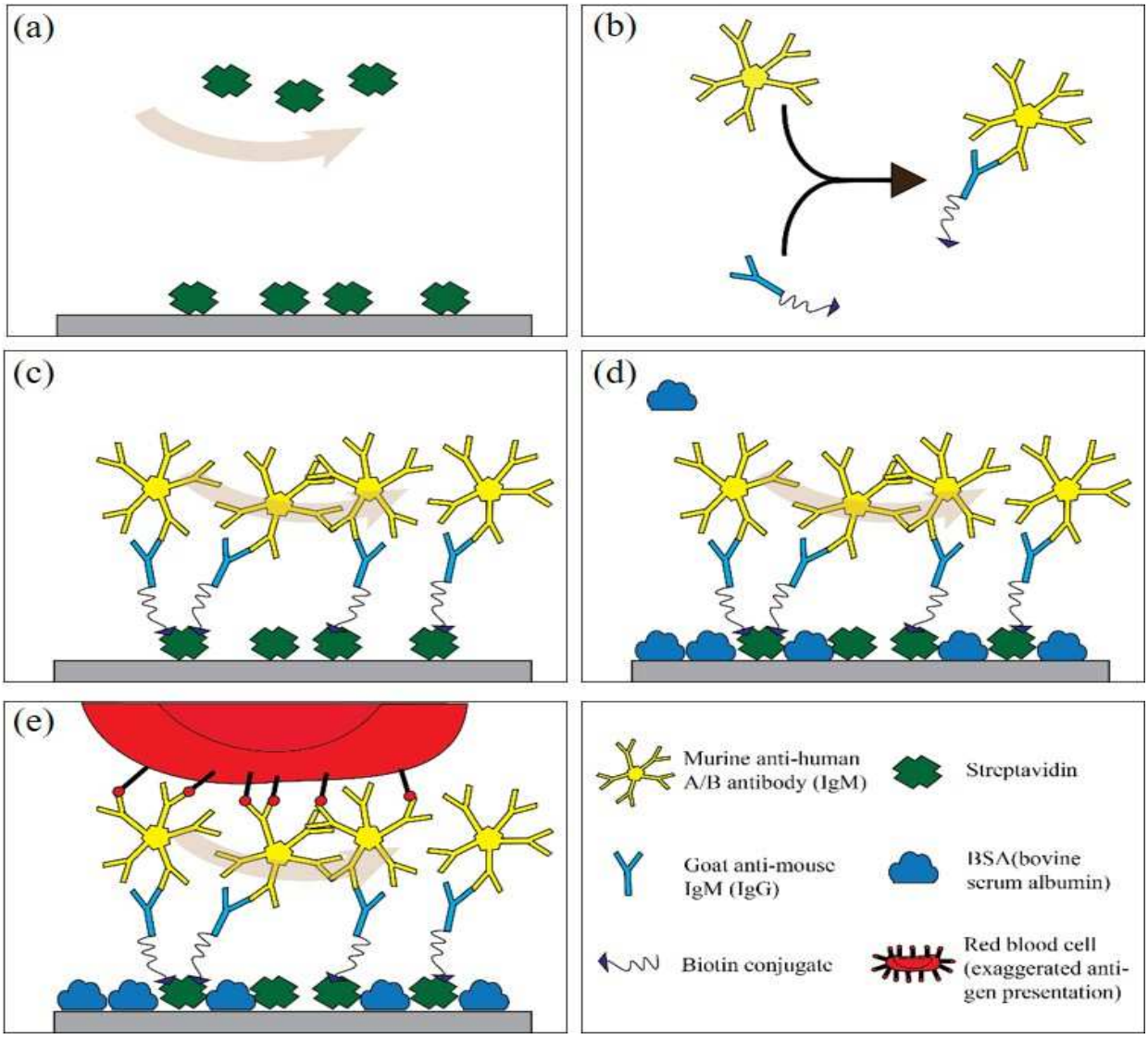

Figure 2-13 Schematic representing the steps involved in the forward typing assay. (a) Streptavidin is passively adsorbed to sensors. (b) Preparation of the capture antibody mix by incubating equal molar of biotinylated anti-mouse IgM and anti-blood group A or B IgM antibody. (c) Binding of the capture antibody mix to the streptavidin coated surface. (d) Blocking any remaining exposed surfaces on the sensor using BSA. (d) Introduction of washed human red blood cells to the sensor and binding of red blood cells to the antibodies. Steps (a)-(d) were conducted off-line while step (e) were performed during the assay.

involved in functionalizing sensors and performing direct typing assays. Methods for sensor functionalization are described in detail in section 2.C.6 and depicted in Fig. 2-13. For direct typing assays, sensors were exposed to diluted, washed human red blood cells followed by a PBS rinse (Fig. 2-10e). Secondary amplification is not required for determining specific outcomes of the assay. Sensor functionalization was accomplished in a similar manner as how the photonic chip was prepared for indirect assay, namely anti-A and anti-B capture antibody mixes were spotted directly on to TE and TM

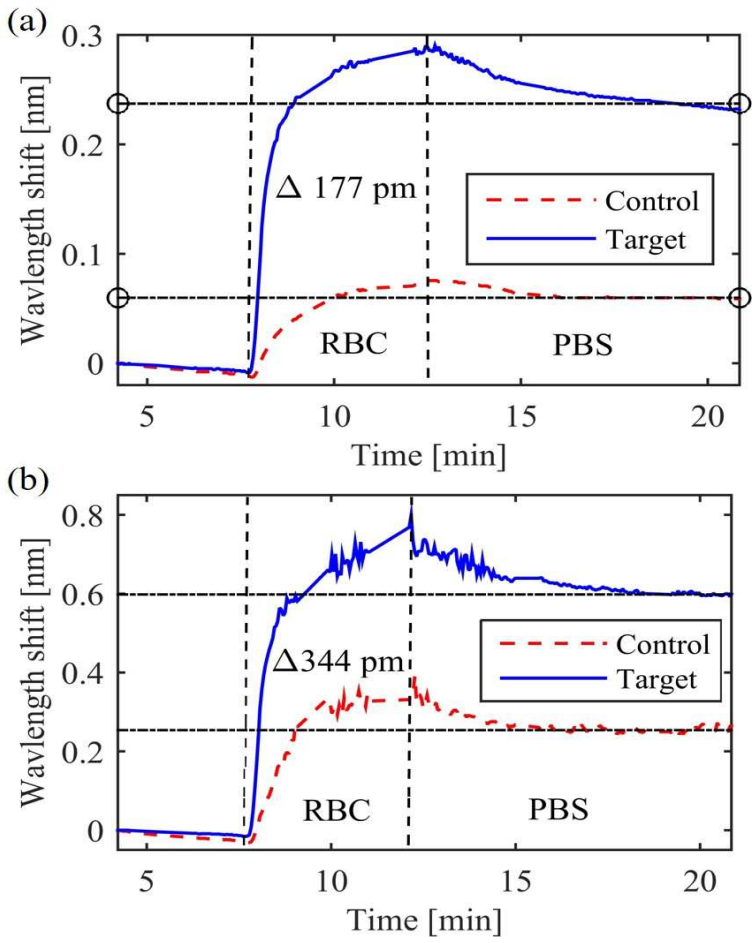

Figure 2-14 Forward typing results of type-A RBCs on (a) TE and (b) TM mode microring resonators functionalized with anti-A antibodies.

mode rings. Since only type A and B erythrocytes were used in the analysis and the number of available rings is limited, either anti-A or anti-B sensors was used as a control for the sample of complimentary ABO blood type. A reference subtraction is performed by subtracting the wavelength shift of the control ring from the wavelength shift of the target ring for analysis. The differential shift suggests the presence of bound blood group antigens on the sensors.

Figures 2-14a and 2-14b show the sensorgrams of direct typing assays on type A erythrocytes using TE and TM mode rings, respectively. Figures 2-15a and 2-15b show the sensorgrams of direct typing assays on type B erythrocytes using TE and TM mode rings, respectively. Overall, the outcomes of direct typing assay are specific and still consistent with indirect typing, as higher resonance wavelength shifts were observed on a TM mode ring than its TE counterpart by approximately two folds. It is worth mentioning that although erythrocytes are significantly larger than protein biomarkers, such as IgG and IgM immunoglobulins, the differential shifts in refractive index measured by the phenotypic typing assay are on par with serologic typing shifts. This equivalent response for the two assays is likely due to the limited penetration depth of the evanescent field and the fact that the sensing surface area of a ring resonator that is less accommodating for whole cells (typically 5-7 microns in diameter, 10-15 fold larger than the width of the waveguide) compared with much smaller biomacromolecules (5-12 nanometers). Erythrocytes can

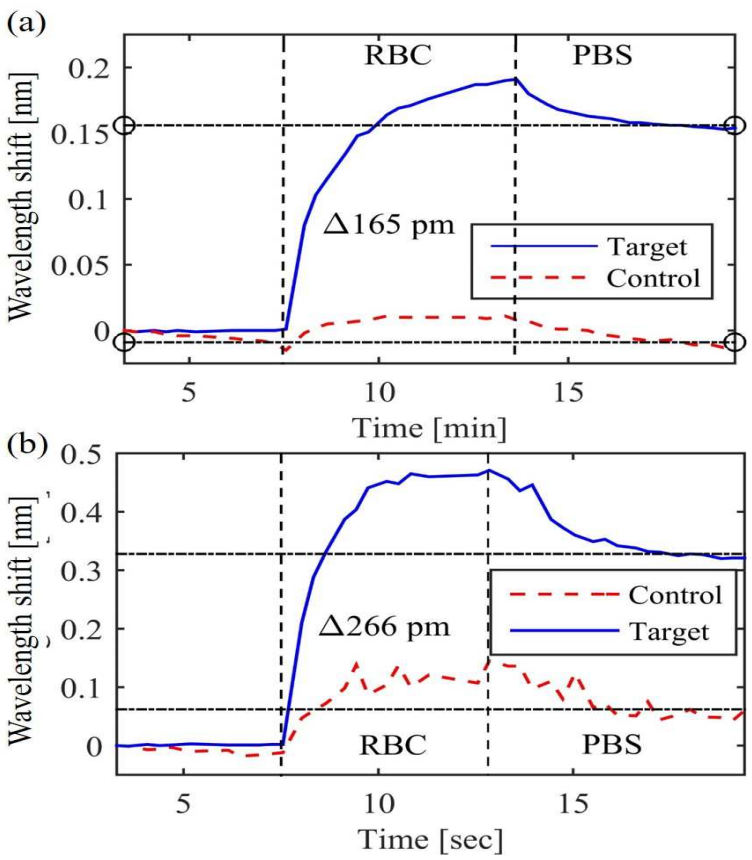

Figure 2-15 Forward typing results of type-B RBCs on (a) TE and (b) TM mode microring resonators functionalized with anti-B antibodies.

bind to the antibody-functionalized photonic chip outside of the sensing region, thereby limiting the total response of the sensor. Figure 2-16 shows an overhead micrograph of the ring resonators exposed to erythrocytes during the assay. The relative size of erythrocyte to the ring resonator is shown in the inset. Another contributing factor for the observed signals is associated with our current protocol that constantly flows cells at 20 μL/min over the sensors without briefly pausing the flow. I t has been shown on SPR that a stop flow could improve the signals compared to those generated during a continuous flow, providing cells sufficient time to bind to the surface[52]. Small pulsating noises on the sensorgrams of Figures 2-14 and 2-15 are exclusively observed in the direct typing assay and may serve as an evidence for how erythrocytes interact with the sensor surface under the flow condition.

2.E Conclusions

This work represents the first side-by-side evaluation of the performance of TE and TM mode ring resonator biosensors for both serologic and phenotypic characterization of human blood. TE and TM mode ring resonators were designed, fabricated, and characterized for use as biosensors. While TE mode rings offer higher intrinsic limits of detection, they are more susceptible to thermal noise than TM mode rings. TM mode rings offer higher sensitivity than TE mode rings because of a larger evanescent field

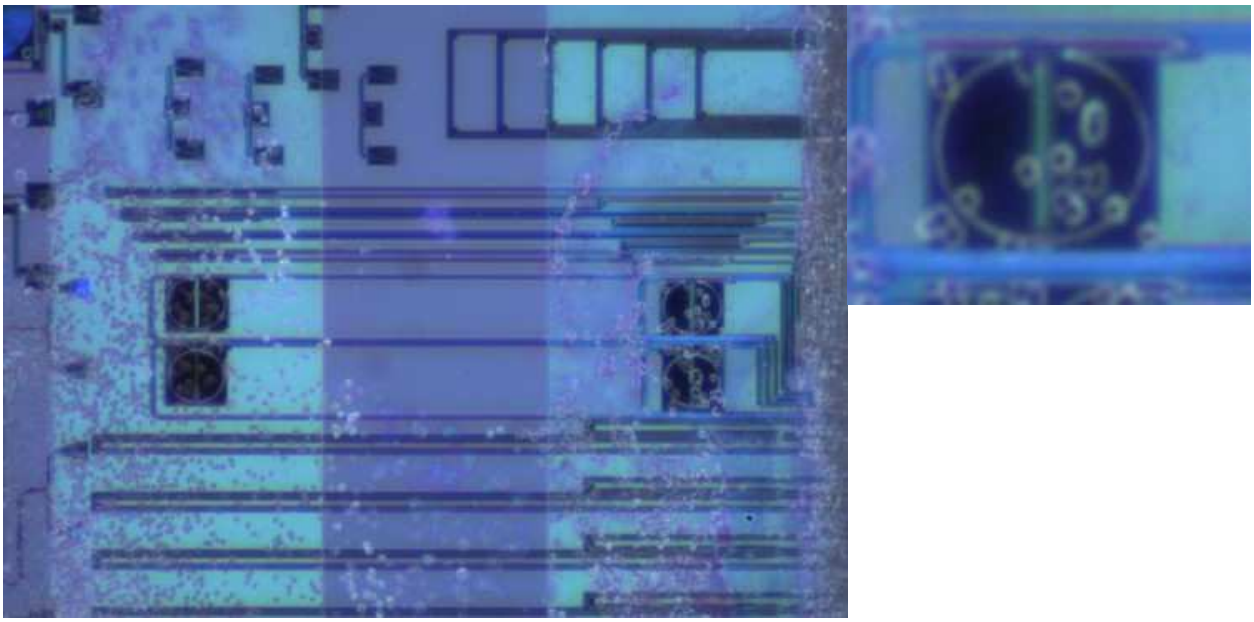

Figure 2-16 An overhead micrograph of the sensors during the forward typing assay. The flow was stopped for taking an image. (Inset) Magnified view showing the relative size of RBCs to an individual ring resonator.

overlap with the surrounding environment, but suffer from a larger absorption loss to the sample. Both types of rings were functionalized for serologic and phenotypic typing assays and in separate assays were monitored under exposure to human plasma and red blood cells. Sensorgram results varied due to differences in human samples, but could be clearly differentiated based on blood type.

To further improve this blood typing system, thin waveguide ring resonators[8] or sub-wavelength grating rings[53] could be used to increase the native surface sensitivity of the biosensors. Additionally, zwitterionic polymer coatings could be used to reduce non-specific protein adsorption[54], which may help increase the operational range of the sensors, especially for samples with low antibody titers. Finally, further investigation of specific capture antibodies and antigens will ensure a robust platform capable of performing across a wide range of samples. We believe this work clearly demonstrates the potential for silicon photonic biosensors for use in blood typing applications, helping to improve the efficiency and utilization of blood products in transfusion medicine.

2.E.1 Study Acknowledgements

We gratefully acknowledge Dr. Sahba Talebi-Fard for her previous work on thin waveguide TE and TM mode ring resonators, Dr. James T. Kirk and Dr. Jing Shang for developing the direct and indirect typing assay protocols, Dr. Jill Johnsen at BloodWorks Northwest for providing human samples, Dr. Andrew Lingley and Duane Irish for cladding chips with CYTOP, and Dr. Nicholas Jaeger for the use of his laser in these experiments.

This work was supported by the University of Washington (UW) Royalty Research Fund, NSF CBET (Award no. 0930411), the Wallace H. Coulter Foundation, and the Washington Research Foundation. We gratefully acknowledge Lumerical Solutions Inc. for providing the simulation software. Fabrication support was provided via the Natural Sciences and Engineering Research council of Canada (NSERC) Silicon Electronic-Photonic Integrated Circuits (SiEPIC) Program. The devices were fabricated by Richard Bojko at the University of Washington Nanofabrication Facility, part of the National Science Foundation's National Nanotechnology Infrastructure Network (NNIN).

Chapter 3. Using Machine Learning and Silicon Photonic Biosensors for Red Blood Cell Characterization

3.A Abstract

Tens of millions of units of blood are transfused worldwide each year, with each individual unit requiring manual typing by a trained technician prior to transfusion. Several tools exist to help expedite the typing process, yet typing still remains a slow and costly process. In an effort to increase throughput and decrease costs of blood typing, recent work involving silicon photonic biosensors has demonstrated their potential as a rapid, low cost tool for typing blood. In this study, we demonstrate the potential for machine learning-based interpretation of photonic blood typing data, providing accurate results without the need for a trained technician. To the best of our knowledge, this is the first demonstration using machine learning to automatically analyze data from silicon photonic microring resonators.

3.B Introduction

3.B.1 ABO and RhD blood typing

Over 100 million units of blood are donated and transfused worldwide every year[55], with over 20 million units in the US alone[56]. Prior to transfusion, the ABO and RhD blood types of the blood of both the donor and the recipient must be determined and matched. If donated blood doesn't match the types of the recipient's blood, hemolytic reactions involving immune and clotting responses can occur, leading to shock, kidney failure, or even death[57]. These hemolytic reactions account for roughly a quarter of transfusion related fatalities. As such, accurate methods for blood typing are a necessity in transfusion medicine.

The current gold standard method for blood typing is based on agglutination between red blood cells and blood group antibodies. Typically performed by highly trained technicians in a clinical laboratory, standard blood typing methods consist of two parts, forward and reverse typing. Forward typing is performed by adding blood group antibodies of known type to diluted red blood cells of

unknown type. Reverse typing is performed by adding reference reagent red blood cells with known surface antigens to diluted plasma containing unknown antibodies. In both tests, the presence of antibodies against the surface antigens expressed on RBCs leads to an agglutination reaction, which is scored semi-quantitatively on a scale of 0 (no agglutination) to 4+ (strong agglutination). While these agglutination assays have the accuracy required for transfusion medicine, they do have several limitations. Both forward and reverse typing are slow, requiring between 30 and 60 minutes for complete agglutination to occur. Typing reagents are expensive, with a full typing panel costing as much as $100 per unit of blood[5]. Also, as measurement of agglutination is non-quantitative, highly trained technicians are required to evaluate the results of testing.

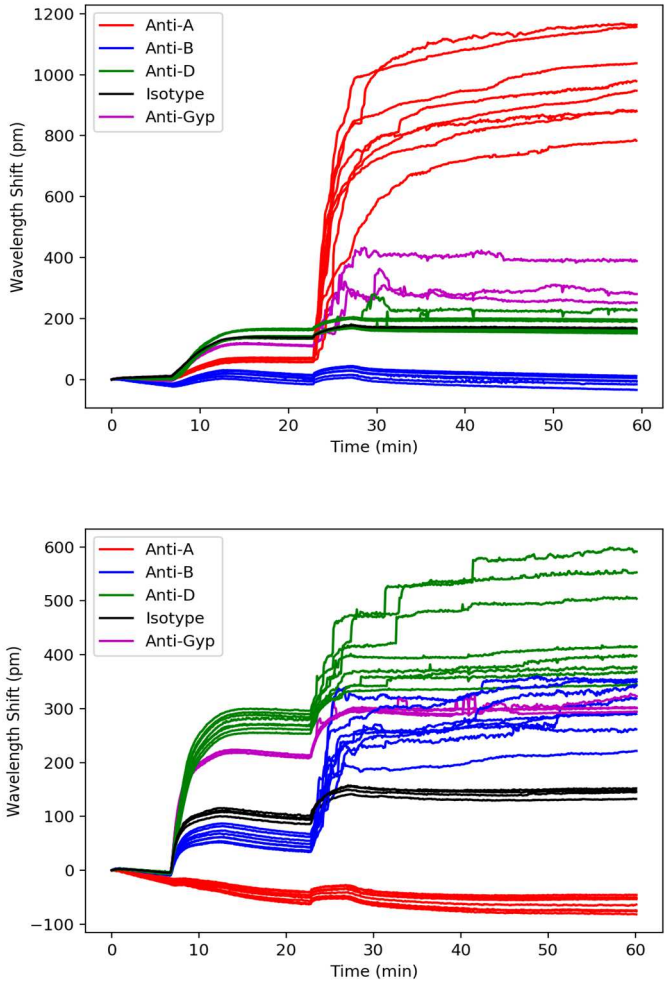

Figure 3-1 Sensorgrams of typical A forward typing results (a) Positive A response, type-A/RhD negative (b) Negative A response, type-B/RhD positive

3.B.2 Silicon photonic biosensors

Silicon photonics is a chip-scale technology that guides near-infrared light in nano-scale silicon wires known as waveguides. While traditionally used by the telecommunications industry, silicon photonics has shown promise recently for biosensing and lab-on-chip systems. These devices operate using electric fields to detect molecular binding events on the surface of waveguides. By adding resonant structures

such as microring resonators, the sensitivity of these devices can be enhanced to a range suitable for detection of various clinical analytes[21-25]. Recent work from Khumwan, et al., has demonstrated a proof-of-concept for using silicon photonic chips for rapid, low-cost, multiplexed forward and reverse blood typing assays[58]. While the demonstrated method addresses several of the current limitations of standard agglutination assays, it still requires a highly trained technician to interpret results. Extensive work has been done to automate the analysis of data from other biosensors using machine learning, including identifying epilepsy using EEG signals[59], detecting arrhythmia from ECG data[60], quantifying output from lateral flow assays[61], and interpreting spectra from surface enhanced Raman spectroscopy[62]. To the best of our knowledge, machine learning has not been used to interpret data from multiplexed silicon photonic biosensors. As such, in this work, we evaluate several machine learning models for automatically

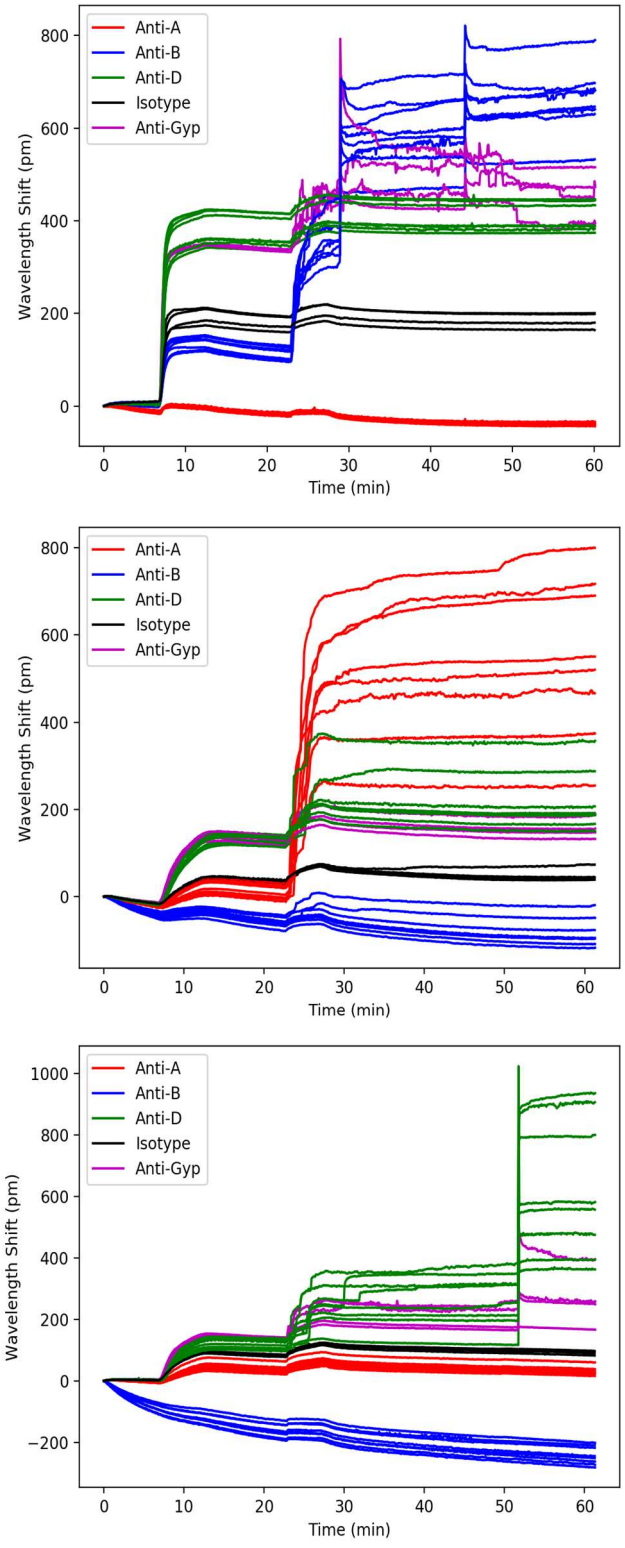

Figure 3-2 Sensorgrams of typical B forward typing results (a) Strong B response, type-B/RhD negative (b) Weak B response, type-AB/RhD positive (c) Negative B response, type-O/RhD positive

producing meaningful results from the data produced by silicon photonic blood typing chips.

3.C Methods and Materials

3.C.1 Data collection

Forward typing assays were performed using IMEC-3 microring resonator chips and Maverick M1 system purchased from Genalyte, Inc., (San Diego, CA). Khumwan, et al., describe the sensor functionalization, sample preparation, and assay protocols in detail[58]. Briefly, chips were passively coated with streptavidin, and biotinylated forward typing reagents were inkjet printed onto sensors by Scienion AG (Princeton, NJ). Blood samples stored in EDTA or citrate were centrifuged and red blood cells were diluted 1:10 in PBS at room temperature. Following an initial PBS rinse, the RBC suspension was flowed over the chip for 5 minutes at 20 µl/min, followed by PBS. For this study, data

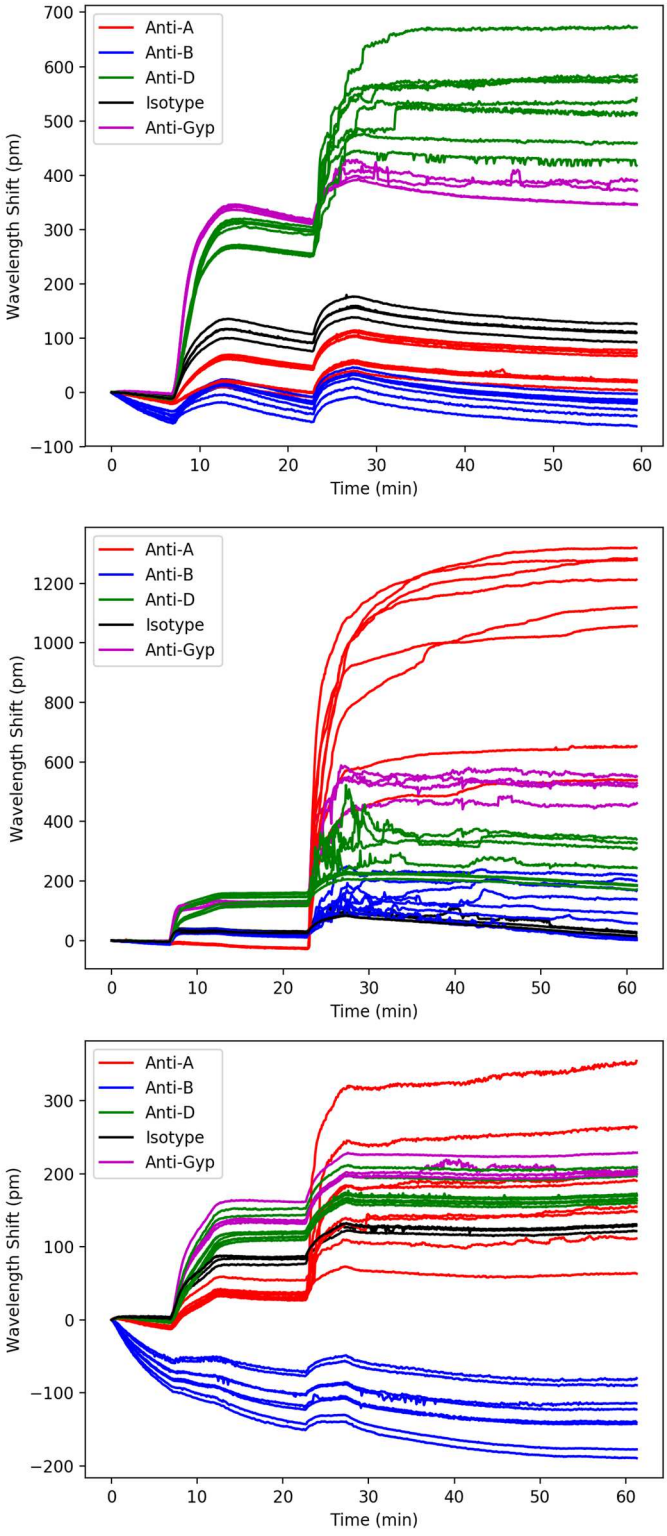

Figure 3-3 Sensorgrams of typical D forward typing results (a) Strong D response, type-O/RhD positive (b) Transient D response, type-AB/RhD negative (c) Negative D response, type-A/RhD negative

from sensors functionalized with anti-A, anti-B, and anti-RhD (n = 8 for each reagent) was used, along with data from sensors functionalized with anti-glycophorin A (n = 4, positive control) and anti-mouse IgM (n = 4, negative control) for a total of 32 sensors. 220 separate blood samples were collected and analyzed, with an even distribution of ABO and RhD types across all samples.

3.C.2 Data preprocessing

Prior to analysis, several data cleaning and preprocessing steps were taken. In several isolated cases, individual sensors may fail to register with the photonic test system or may fail to produce a strong resonance peak. Across all sensors used in this study, 52 (out of over 7000) sensors had such failures and were removed from analysis. In these cases, missing values were imputed with the pointwise average signal of the remaining sensors in the local cluster of four sensors with the same functionalization. No chip had more than 4 failed sensors across all sensor clusters, and no chip had any completely failed clusters. After failed sensors were imputed, the pointwise average signal for the negative control sensors (anti-mouse IgM) was calculated for each chip. Data was normalized across all chips by subtracting the negative control average from each sensor on each chip and then dividing all data points by the maximum signal value on each chip.

To quantify the high-frequency components of RBC binding signals observed by Khumwan, et al., one-dimensional local binary patterns (1D-LBPs) were calculated for each sensor[58]. LBPs were calculated as described in Kaya, et al., with 4 neighbor points on either side of a center point with the value of the center point used as the binary threshold for each neighbor point. After the LBP value was calculated for each sensor, a 256-bin histogram of LBP values was generated for each sensor for use as a dimensionally reduced feature set.

3.C.3 Computational analysis

Following preprocessing and feature extraction, several different learning models were used as binary classifiers to separately predict the presence or absence of the A, B, and D blood group antigens. Support

vector machines (SVMs), decision trees (DTs), random forest classifiers (RFCs), and multilayer perceptrons (MLPs) were separately evaluated for overall accuracy, specificity, and sensitivity when trained and validated on either preprocessed data or 1D-LBP histograms generated from preprocessed data. Unless otherwise stated, hyperparameter optimization was performed using 5-fold cross-validation. A, B, and D types for each sample were provided by Bloodworks Northwest and used as data labels.

SVM Hyperparameter Optimization: A cross-validated grid search of two hyperparameters (kernel, C) was performed. Linear, polynomial (degree = 3), RBF (radial basis function, gamma = 1 / number of features), and sigmoid kernels were tested along with values of C spanning 6 orders of magnitude (0.001 to 100).

DT Hyperparameter Optimization: A cross-validated grid search of two hyperparameters (maximum depth, minimum samples per leaf) was performed. All integer values between 2 and 10 were tested for both parameters.

RFC Hyperparameter Optimization: A cross-validated grid search of three hyperparameters (maximum depth, minimum samples per leaf, and minimum samples per split) was performed. Maximum depth values between 2 and 25 were tested. Values between 1 and 32 were considered for both minimum sample parameters.

MLP Optimization: Models with either one or two hidden layers (HL) of varying sizes were evaluated with 10-fold cross validation. Batch normalization and dropout layers were included between hidden and output layers. All hidden layers used rectified linear unit (ReLU) activation functions and the output layer used softmax activation.

3.D Results and Discussion

Following model optimization, leave-one-out cross validation (LOOCV) was used to find the overall accuracies, specificities, and sensitivities of each optimized model. Using the hyperparameters and network structures selected during optimization, each model was trained with 219 preprocessed raw data

samples and used to predict the A, B, and D types of the remaining sample. This process was repeated until all 220 samples had type predictions from every model (Table 3-1). The same process was also completed using 1D-LBP histograms as inputs instead of preprocessed raw data.

3.D.1 Preprocessed raw data results

Across all three typing classifications (A, B, and D), neural networks generally stood out as the most accurate model. For A typing, both 1 and 2 HL MLPs tied for the highest accuracy of any model, 97.3%. For B typing, the 1-HL MLP tied with the SVM for the highest accuracy (82.7%), with the 2-HL MLP coming in second at 81.4%. The 2-HL MLP performed best in D typing, with an overall accuracy of 91.8%. Decision trees consistently had the lowest accuracy of any model, likely due to the simplicity of the model relative to the complexity of the data. While decision trees did have low overall accuracies, it is worth noting that the B and D decision trees were the only two models with higher sensitivities than specificities. Independent of type, the top performing models had specificities between 95 and 100% with lower sensitivities making up for most of the difference in overall accuracy.

As observed by Khumwan, et al., A, B, and D all have similar features indicating a positive test (large signal amplitude, high-frequency noise content), but B and D tend to have wider variance in the strength of these features[58]. In A typing, positive and negative signals tend to be very distinct, as shown in Figure 3-1. By comparison, B typing often has weak positives that can be easily confused by both humans and computational models as negative results (Figure 3-2). D typing tends to have less weak positives than B, but more than A. There is also a special type of negative signal in D typing where the sensors appear to be responding positively in the first half of a test, then stop responding in the second half (Figure 3-3). These “transient” D responses are often confused with weak positives, which has the effect of increasing the number of false negatives predicted both algorithmically and by hand.

Table 3-1 Typing accuracy, specificity and sensitivity by antigen type and by model

A Antigen	**Accuracy**	**Specificity**	**Sensitivity**
SVM	96.8%	100%	93.6%
DT	94.1%	94.5%	93.6%
RFC	96.4%	99.1%	93.6%
1-HL MLP	97.3%	100%	94.5%
2-HL MLP	97.3%	100%	94.5%
B Antigen			
SVM	82.7%	99.1%	66.4%
DT	79.5%	78.2%	80.9%
RFC	79.5%	83.4%	75.5%
1-HL MLP	82.7%	94.5%	70.9%
2-HL MLP	81.4%	83.4%	79.1%
D Antigen			
SVM	89.5%	95.5%	83.6%
DT	77.3%	76.4%	78.2%
RFC	87.3%	91.8%	82.7%
1-HL MLP	90.0%	94.5%	85.5%
2-HL MLP	91.8%	97.3%	86.4%

3.D.2 1D-LBP histogram results

Compared with classification results using processed data as inputs, LBP histogram-based classification has lower accuracy for A, B, and D across all models, except for the A decision tree (both have 94.1% accuracy). The sensitivities and specificities of almost all LBP histogram models are also lower than their processed data equivalents. B DTs, RFCs, and 1-HL MLPs have slightly higher specificities (2-5%) when using LBP histograms.

While LBPs do capture local fluctuations due to high frequency content in a signal, their binary encoding loses information about signal amplitude, which is the other notable feature in the sensor data. As such, the LBP for a signal neighborhood with small fluctuations due to random noise may be the same as a neighborhood with large fluctuations due to high frequency signal content, which can lead to increased numbers of both false positives and false negatives. The only apparent benefit of 1D-LBPs is that they may be slightly better at differentiating weak positive B responses from negative B responses. However, the increased number of false positives more than offsets this improvement, with overall accuracy decreasing.

3.D.3 Potential improvements

Two main classes of limitations currently exist for the demonstrated method of blood typing. The first is the chemistry of the assay itself. Khumwan, et al., address a decrease in typing accuracy on older chips, suggesting that capture efficiency decreases over time[58]. There is also a need for further optimization of reagent immobilization techniques and investigation of capture antibodies with higher antigen specificity (especially anti-B and anti-RhD). Separate from the assay chemistry, there are several issues with the data analysis itself. The most immediate limitation to algorithmic analysis is the number of samples available to train with. Especially for neural network-based approaches, more training examples are expected to directly improve accuracy. Additionally, improved feature extraction and dimensionality reduction may also improve typing results. Approaches that capture both amplitude and frequency information with a reduced number of features likely will reduce training complexity and improve

classification accuracy. Finally, accuracy may be further improved via ensemble learning such as a voting classifier. In cases where individual samples are classified differently by different models, a voting classifier has the potential to improve accuracy by taking into account the predictions from several different models.

3.E Conclusions

Silicon photonic biosensors have shown promise for use as a rapid, highly multiplexed, and point-of-care diagnostic platform for blood typing[58]. However, silicon photonic blood typing assays still have the limitation of requiring a specially trained technician to accurately interpret test results. Here, we have demonstrated the potential of machine learning for greatly simplifying this analysis. In addition, we have also identified multiple potential techniques for further improving automated analysis accuracies. We also acknowledge the need for larger sample sizes for improving model accuracy and reliability. Despite the current limitations however, the computational results are nearing the accuracy of human interpretation of the same assays, and are expected to exceed human accuracies once larger sample sizes are available and improved feature extraction methods are implemented.

3.E.1 Study acknowledgements

We would like to thank Bloodworks Northwest for facilitating and organizing sample acquisition, distribution and management as well as Dr. Nathan Kutz for his assistance with selecting methods for computational analysis. This proof-of-concept work is supported by the Life Sciences Discovery Fund (LSDF), the Wallace H. Coulter Foundation, and the National Science Foundation (NSF).

Chapter 4. Overall Conclusions and Future Directions

The studies performed in this thesis focus on evaluating the potential of multiple different technologies to be used in the development of rapid, low cost blood typing diagnostics. Transverse electric (TE) and transverse magnetic TM mode microring resonators were compared for forward and reverse typing assays involving the ABO system. Both types of sensors demonstrated adequate sensitivity for blood typing applications and both come with several advantages of silicon photonic biosensors over traditional blood typing assays. Both sensors are cheap to manufacture and use significantly smaller volumes of reagents than tube typing assays. Also, neither sensor requires the incubation time that a standard agglutination assay requires, giving the potential for a much faster assay. When compared against each other, TM mode sensors tend to have stronger responses in both forward and reverse typing than TE mode sensors exposed to the same blood sample. The stronger TM response is likely due to the increased evanescent field overlap with the analytes. In order to fully confirm the improved performance of TM mode sensors, more samples would need to be tested on both TE and TM mode sensors, but this preliminary work suggests that TM mode sensors may be better suited to blood typing applications.

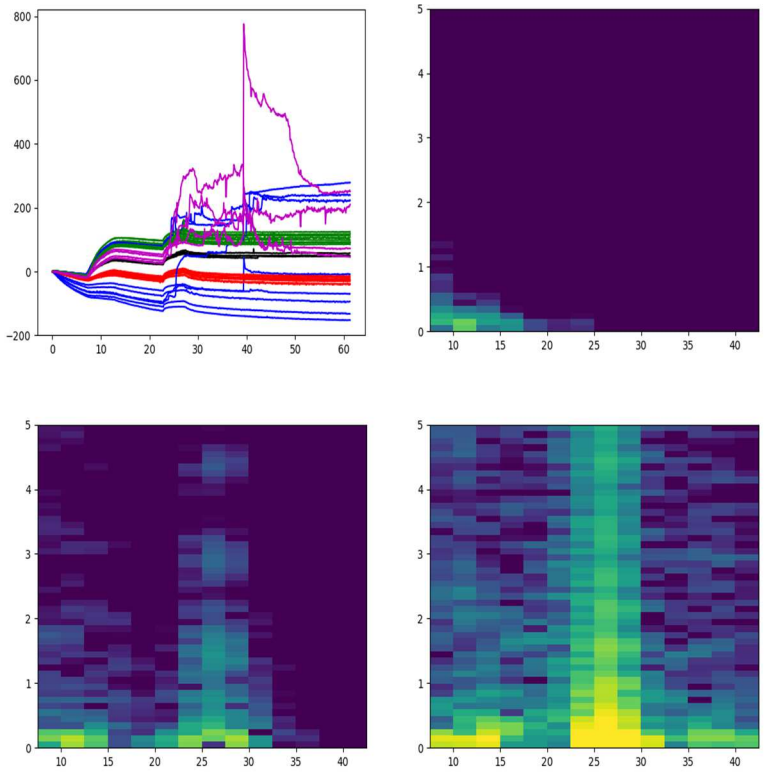

Figure 4-1 Sprectrograms of forward typing data from a B-negative sample (a) raw data sensorgram (b) spectrogram of negative response (anti-A, shown in red). (c) spectrogram of weak positive response (anti-B, shown in blue). (d) spectrogram of strong positive response (anti-Gly, shown in magenta).

The other technology evaluated for use with silicon

photonic blood typing assays was machine learning. With the recent increase in number of readily accessible machine learning toolkits, it is easier than ever before to rapidly develop accurate and user-friendly analysis algorithms for biosensing assays. Data from a recent proof-of-concept study[58] using highly multiplexed silicon photonic blood typing chips to type over 200 human blood samples was used to train, optimize, and evaluate several different machine learning algorithms for predicting blood type from biosensor data sets. These early results are promising, as multiple different models had accuracies rivaling the by-hand analysis from the previous study. Multiple limitations were present in this work, including a small sample size relative to most machine learning studies, and a lack of robust feature extraction. However, at least one additional promising feature set has already been suggested since the analysis was completed. Since forward typing data is known to contain meaningful high-frequency content, 2D spectrograms of each signal have been proposed as a calculated feature that captures frequency information without sacrificing amplitude data (Figure 4-1). As spectrograms and other feature extraction methods are tested and more blood samples are tested, automated typing accuracies should continue to increase and surpass the standard by-hand analysis.

References

1. Speiser, Paul, and Ferdinand G. Smekal. *Karl Landsteiner: the discoverer of the blood-groups and a pioneer in the field of immunology; biography of a Nobel price winner of the Vienna medical school*. Hollinek, 1975.
2. Schwarz, Hans Peter, and Friedrich Dorner. "Karl Landsteiner and his major contributions to haematology." *British Journal of Haematology* 121.4 (2003): 556-565.
3. Storry, Jill R., and Martin L. Olsson. "Genetic basis of blood group diversity." *British journal of haematology* 126.6 (2004): 759-771.
4. Reid, Marion E., Christine Lomas-Francis, and Martin L. Olsson. *The blood group antigen factsbook*. Academic press, 2012.
5. Forbes, J. M., et al. "Blood transfusion costs: a multicenter study." *Transfusion* 31.4 (1991): 318-323.
6. Taswell, H. F., L. L. Nicholson, and M. L. Cochran. "Automated blood typing of patients." *Transfusion* 14.2 (1974): 124-129.
7. Bogaerts, Wim, et al. "Silicon microring resonators." *Laser & Photonics Reviews* 6.1 (2012): 47-73.
8. Schmidt, Shon, et al. "Improving the performance of silicon photonic rings, disks, and Bragg gratings for use in label-free biosensing." *Biosensing and Nanomedicine VII*. Vol. 9166. International Society for Optics and Photonics, 2014.
9. Wang, Xu, et al. "A silicon photonic biosensor using phase-shifted Bragg gratings in slot waveguide." *Journal of biophotonics* 6.10 (2013): 821-828.
10. Flueckiger, Jonas, et al. "Cascaded silicon-on-insulator microring resonators for the detection of biomolecules in PDMS microfluidic channels." *Microfluidics, BioMEMS, and Medical Microsystems IX*. Vol. 7929. International Society for Optics and Photonics, 2011.
11. Kirk, James Thomas. *Silicon Photonic Biosensors for the Phenotypic and Serologic Characterization of Blood*. Diss. 2015.
12. Vlasov, Yurii. "Silicon photonics for next generation computing systems." *European Conference on Optical Communications*. 2008.
13. Rickman, Andrew. "The commercialization of silicon photonics." *Nature Photonics* 8.8 (2014): 579.
14. Soref, Richard. "Silicon photonics: a review of recent literature." *Silicon* 2.1 (2010): 1-6.
15. Fan, Xudong, et al. "Sensitive optical biosensors for unlabeled targets: A review." *analytica chimica acta* 620.1-2 (2008): 8-26.
16. Jokerst, Nan, et al. "Chip scale integrated microresonator sensing systems." *Journal of biophotonics* 2.4 (2009): 212-226.
17. Barrios, Carlos Angulo. "Integrated microring resonator sensor arrays for labs-on-chips." *Analytical and bioanalytical chemistry* 403.6 (2012): 1467-1475.
18. Jokerst, Nan Marie, et al. "Progress in chip-scale photonic sensing." *IEEE transactions on biomedical circuits and systems* 3.4 (2009): 202-211.
19. Fernández Gavela, Adrián, et al. "Last advances in silicon-based optical biosensors." *Sensors* 16.3 (2016): 285.
20. Vörös, Janos. "The density and refractive index of adsorbing protein layers." *Biophysical journal* 87.1 (2004): 553-561.
21. Luchansky, Matthew S., and Ryan C. Bailey. "Silicon photonic microring resonators for quantitative cytokine detection and T-cell secretion analysis." *Analytical chemistry* 82.5 (2010): 1975-1981.
22. Vollmer, Fea, et al. "Protein detection by optical shift of a resonant microcavity." *Applied physics letters* 80.21 (2002): 4057-4059.

23. Suter, Jonathan D., et al. "Label-free quantitative DNA detection using the liquid core optical ring resonator." *Biosensors and Bioelectronics* 23.7 (2008): 1003-1009.
24. Vollmer, F., S. Arnold, and D. Keng. "Single virus detection from the reactive shift of a whispering-gallery mode." *Proceedings of the National Academy of Sciences* 105.52 (2008): 20701-20704.
25. Ramachandran, A., et al. "A universal biosensing platform based on optical micro-ring resonators." *Biosensors and Bioelectronics* 23.7 (2008): 939-944.
26. Storry, J. R., and Martin L. Olsson. "The ABO blood group system revisited: a review and update." *Immunohematology*25.2 (2009): 48.
27. Vamvakas, Eleftherios C., and Morris A. Blajchman. "Blood still kills: six strategies to further reduce allogeneic blood transfusion-related mortality." *Transfusion medicine reviews*24.2 (2010): 77-124.
28. Malomgré, Wim, and Birgid Neumeister. "Recent and future trends in blood group typing." *Analytical and bioanalytical chemistry* 393.5 (2009): 1443-1451.
29. Chung, Koo‐Whang, et al. "Declining blood collection and utilization in the United States." *Transfusion* 56.9 (2016): 2184-2192.
30. Kourout, Moussa, et al. "Multiplex detection and identification of viral, bacterial, and protozoan pathogens in human blood and plasma using a high‐density resequencing pathogen microarray platform." *Transfusion* 56.6pt2 (2016): 1537-1547.
31. Quinn, John G., et al. "Detection of blood group antigens utilising immobilised antibodies and surface plasmon resonance." *Journal of immunological methods* 206.1-2 (1997): 87-96.
32. Krupin, Oleksiy, Chen Wang, and Pierre Berini. "Selective capture of human red blood cells based on blood group using long-range surface plasmon waveguides." *Biosensors and Bioelectronics* 53 (2014): 117-122.
33. Houngkamhang, Nongluck, et al. "ABO blood-typing using an antibody array technique based on surface plasmon resonance imaging." *Sensors* 13.9 (2013): 11913-11922.
34. Bonanno, Lisa M., and Lisa A. DeLouise. "Whole blood optical biosensor." *Biosensors and Bioelectronics* 23.3 (2007): 444-448.
35. Liu, Zhugong, et al. "Extended blood group molecular typing and next-generation sequencing." *Transfusion medicine reviews* 28.4 (2014): 177-186.
36. Boccoz, S. A., L. J. Blum, and C. A. Marquette. "DNA biosensor/biochip for multiplex blood group genotyping." *Methods* 64.3 (2013): 241-249.
37. Chester, M. Alan, and Martin L. Olsson. "The ABO blood group gene: a locus of considerable genetic diversity." *Transfusion medicine reviews* 15.3 (2001): 177-200.
38. Hanif, Raza. *Microfabrication of Plasmonic Biosensors in CYTOP Integrating a Thin SiO2 Diffusion and Etch-barrier Layer*. Diss. Université d'Ottawa/University of Ottawa, 2011.
39. Luchansky, Matthew S., et al. "Characterization of the evanescent field profile and bound mass sensitivity of a label-free silicon photonic microring resonator biosensing platform." *Biosensors and Bioelectronics* 26.4 (2010): 1283-1291.
40. Höök, Fredrik, et al. "A comparative study of protein adsorption on titanium oxide surfaces using in situ ellipsometry, optical waveguide lightmode spectroscopy, and quartz crystal microbalance/dissipation." *Colloids and Surfaces B: Biointerfaces* 24.2 (2002): 155-170.
41. Chrostowski, Lukas, et al. "Silicon photonic resonator sensors and devices." *Laser Resonators, Microresonators, and Beam Control XIV*. Vol. 8236. International Society for Optics and Photonics, 2012.
42. Hu, Juejun, et al. "Design guidelines for optical resonator biochemical sensors." *JOSA B* 26.5 (2009): 1032-1041.
43. White, Ian M., and Xudong Fan. "On the performance quantification of resonant refractive index sensors." *Optics express* 16.2 (2008): 1020-1028.
44. Elwing, Hans. "Protein absorption and ellipsometry in biomaterial research." *Biomaterials* 19.4-5 (1998): 397-406.

45. Biosensor, A. Porous Silicon Optical. "Detection of Reversible Binding of IgG to a Protein A-Modified Surface Dancil, Keiki-Pua S.; Greiner, Douglas P.; Sailor, Michael J." *Journal of the American Chemical Society* 121.34 (1999): 7925-7930.
46. Erickson, Harold P. "Size and shape of protein molecules at the nanometer level determined by sedimentation, gel filtration, and electron microscopy." *Biological procedures online* 11.1 (2009): 32.
47. Coen, Martine Collaud, et al. "Adsorption and bioactivity of protein A on silicon surfaces studied by AFM and XPS." *Journal of colloid and interface science* 233.2 (2001): 180-189.
48. Munn, E. A., L. Bachmann, and A. Feinstein. "Structure of hydrated immunoglobulins and antigen-antibody complexes. Electron microscopy of spray-freeze-etched specimens." *Biochimica et Biophysica Acta (BBA)-Protein Structure* 625.1 (1980): 1-9.
49. Darst, Seth A., et al. "Two-dimensional crystals of streptavidin on biotinylated lipid layers and their interactions with biotinylated macromolecules." *Biophysical Journal* 59.2 (1991): 387-396.
50. Weisenhorn, A. L., et al. "Streptavidin binding observed with an atomic force microscope." *Ultramicroscopy* 42 (1992): 1125-1132.
51. Chrostowski, Lukas, and Michael Hochberg. *Silicon photonics design: from devices to systems*. Cambridge University Press, 2015.
52. Pipatpanukul, C., et al. "Microfluidic PMMA-based microarray sensor chip with imaging analysis for ABO and RhD blood group typing." *Vox sanguinis* 110.1 (2016): 60-69.
53. Yousuf, Soha, et al. "Suspended microring resonator sensor using internal sub-wavelength grating." *Optical Sensors*. Optical Society of America, 2015.
54. Kirk, James T., et al. "Zwitterionic polymer-modified silicon microring resonators for label-free biosensing in undiluted humanplasma." *Biosensors and Bioelectronics* 42 (2013): 100-105.
55. World Health Organization. "The 2016 global status report on blood safety and availability." (2017).
56. Whitaker, Barbee, et al. "Trends in United States blood collection and transfusion: results from the 2013 AABB blood collection, utilization, and patient blood management survey." *Transfusion* 56.9 (2016): 2173-2183.
57. Dean, Laura. *Blood groups and red cell antigens*. National Center for Biotechnology Information, 2005.
58. Khumwan, P., et al, "Simultaneous forward and reverse blood typing on multiplexed microring resonator arrays. " *Pending publication*
59. Kaya, Yılmaz, et al. "1D-local binary pattern based feature extraction for classification of epileptic EEG signals." *Applied Mathematics and Computation* 243 (2014): 209-219.
60. Guvenir, H. Altay, et al. "Supervised machine learning algorithm for arrhythmia analysis." *Computers in cardiology*(1997): 433-436.
61. Zeng, Nianyin, et al. "Deep belief networks for quantitative analysis of a gold immunochromatographic strip." *Cognitive Computation* 8.4 (2016): 684-692.
62. Dong, Ronglu, et al. "Detection and direct readout of drugs in human urine using dynamic surface-enhanced Raman spectroscopy and support vector machines." *Analytical chemistry* 87.5 (2015): 2937-2944.